Surface activity of Janus particles adsorbed atfluid-fluid interfaces: Theoretical and experimental aspects.

Miguel Angel Fernandez-Rodriguez, Miguel Angel Rodriguez-Valverde, Miguel Angel Cabrerizo-Vilchez, and Roque Hidalgo-Alvarez*

Biocolloid and Fluid Physics Group, Applied Physics Department, Faculty of Sciences,University of Granada, 18071-E Granada, Spain.

e-mail: rhidalgo@ugr.es

ABSTRACT

Since de Gennes coined in 1992 the term Janus particle (JP), there has been a continued effort to develop this field. The purpose of this review is to present the most relevant theoretical and experimental results obtained so far on the surface activity of amphiphilic JPs at fluid interfaces. The surface activity of JPs at fluid-fluid interfaces can be experimentally determined using two different methods: the classical Langmuir balance or the pendant drop tensiometry. The second method requires much less amount of sample than the first one, but it has also some experimental limitations. In all cases collected here the JPsexhibited a higher surface or interfacial activity than the corresponding homogeneous particles. This reveals the significant advantage of JPs for the stabilization of emulsions and foams.

PACS:
82.70 Dd
68.18-g, 68.47 Pe
68.03-g
68.18 Fg
89.75 Kd
64.75 Xc
75.75 Fk

Keywords: Janus particles; Surface and Interfacial activity; Fluid-fluid interfaces; Particle-laden interfaces; Pendant drop tensiometry.

Contents

1. Introduction

Janus Particles (JPs), named after the double-faced Roman god, are anisotropic colloids with two spatial domains of different physicochemical properties [1]. The contrast between the spatial domains can induce spontaneous self-assembly of the nanoparticles and be responsive to external stimuli such as magnetic or electric fields, pH or temperature gradients [2-4]. Depending on the particular Janus character of the nanoparticles, they cover a wide range of applications such as biosensors, drug-delivery and immunotherapy [5-9], water-repellent textile [10], photonic micro-scale elevator [11] or nanoparticles that become aligned by an external electric or magnetic field [12-19].

In recent years, there is an increasing interest in the design and synthesis of JPs and their self-assembly and physical properties in particle-laden interfaces [20-28]. The JPs are being developed to be used in electronic paper, asymmetrical carriers for catalysis, sensing and drug delivery, nanoscale machinery in the conversion of solar energy into electrical current, colloidal surfactants [29]. More explicitly the JPs laden-interfaces have currently applications as artificial antigen-presenting cells for T-cell activation [30], and in the fabrication of superhydrophobic surfaces formed by micropillars with hydrophobic sidewalls and hydrophilic tops, which are Janus micropillars [10].

One of the most fascinating applications of JPs is the stabilization of multiphasic fluid mixtures such as emulsions and bubbles because these particles are adsorbed to the interfaces more efficiently than their homogeneous counterparts [25,31-33]. To develop these applications it is mandatory to evaluate properly the colloidal stability in bulk and the interfacial activity of JPs and their interplay. However, there are a few woks devoted to study these properties. Glaser et al. were the first to measure the interfacial activity of JPs (composed of gold and an iron oxide moiety) at liquid-liquid interfaces (water-hexane) by using pendant drop tensiometry [28]. Casagrande et al. [25] performed the first experiments on the behavior of JPs at water-oil interfaces, but they only focussed their experiments on the position of particles at that interface. Most recently, Ruhland et al. [34] have performed the first study on the self-assembly behavior of Janus cylinders at liquid-liquid interfaces using pendant drop technique and microscopic imaging. Kumar et al. [26] have published a review on amphiphilic JPs at fluid interfaces where they survey the recent development in the use of these particles as colloidal surfactants to stabilize multiphasic mixtures such as emulsions. They also discuss on the importance of controlling the shape of JPs, which has a significant impact on their behaviour at fluid interfaces. Obviously, the area occupied by the JPs at the interface changes drastically as they aggregate because they lose their original size and shape. Ruhland et al. [34] were the first in describing an experimental study on the self-assembly of Janus cylinders at liquid interfaces. These authors found significant differences in the structures formed at the interface. More recently, the same authors have studied again the influence of JP shape on their interfacial behavior at liquid-liquid interfaces [35]. More

specifically they investigated the self-assembly behavior of JPs with different geometries (spheres, cylinders and discs) trapped at an oil-water interface.

JPs with wettability anisotropy can be used to stabilize Pickering emulsions during longer periods of time and under experimental conditions more stressing (temperature changes or shear effects, for instances) than with homogeneous particles (HPs). Unlike HPs, amphiphilic JPs can exhibit high interfacial activity regardless of the degree of amphiphilicity, due to the spatial separation of the different wettability regions [31]. Thus, amphiphilic Janus-like gold nanoparticles functionalized with thiol-terminated polyethylene glycol chains and short alkane-thiols have been used as water/oil emulsion stabilizers because the authors state that the domains rearrange when the JPs are placed at the interface [36]. However, recently Reguera et al. [37] found that the capping ligands of gold nanoparticles functionalized with 1-octanethiol and 6-mercapto-1-hexanol did not rearrange when placed at a fluid-fluid interface. Moreover, gold JPs half functionalized with polydopamine show that the electrostatic repulsion between nanoparticles determine the resulting particle self-assembly at water/oil interfaces as a result of the hydrophilic polydopamine and hydrophobic gold faces of each particle [38]. In addition, micrometer-sized gold-silica JPs have been found to stabilize water/oil emulsions for longer than one year, compared to 2h of demulsification when homogeneous silica nanoparticles were used [39]. Importantly, not only the wettability contrast of the JPs rules the interfacial activity, their morphology also controls the interfacial activity at a given water/oil interface, which determines the packing behavior of the JPs [35]. Thereby, nonspherical drops of emulsion have been obtained by using asymmetrical JPs [40].

There are different synthesis strategies involving bulk methods in which the JPs are synthesized in a solvent, usually *one-pot* method [13,36,41]. On the other hand, in other strategies the particles are trapped at a given liquid interface to be functionalized [27,42], usually resulting in noticeably lower amount of JPs than in bulk methods. It should be noted that the details on the synthesis of JPs are out of focus of the aims of this review. Recently, some reviews on the JP synthesis have been published [24,25].

Characterization of the surface activity of JPs is of fundamental interest as they represent a completely new class of Pickering surfactants [26]. The surface characterization of colloidal monolayers formed by JPs becomes a difficult task [43,44]. To explore the surface activity of spherical JPs at fluid interfaces, the following factors are crucial: the colloidal stability of the particles in bulk, the presence of traces of the surface-active reagents used in the particle synthesis and of the spreading agent typically employed to prepare colloidal monolayers. These factors may hinder the effect of the interface area on the surface pressure due exclusively to the presence of JPs. The extremely low colloidal stability of JPs is a serious limitation in their utilization as colloidal surfactants. Park *et al.* [45] have studied the self-assembly behaviour of JPs at fluid interfaces in detail. These authors found that JPs form a fractal-like aggregate structure spontaneously, which means that their interactions are

predominantly attractive. The formation of aggregates at fluid interfaces makes unrealizable the study of colloidal monolayers, because these aggregates lead to multilayers or unresolved monolayers. Nie et al. [46] found that amphiphilic polymeric JPs assembled into supermicelles. Chen et al. [47] found that JPs with a hydrophobic hemisphere and a negatively charged hemisphere aggregate in supracolloidal objects ranging from spherical clusters to fibrillar triple helices. Furthermore, it has been reported that metallo-dielectric JPs form fibrillar-like shapes under external electric or magnetic fields [12-18]. Yu et al. [48] found similar fibres external field but by preferential wetting of the hemispheres of silica and gold JPs. Shah et al. [49] reported that the fibres formed by metallo-dielectric Janus ellipsoids under AC electric field kept a shape-memory of the state before the external field is applied. From simulations, Beltran-Villegas et al. [50] found that Janus spheres under sedimentation form lamellar structures. Instead, as reported by Luo et al. [51], a stable colloidal monolayer can be formed with electrically charged JPs. Simulations performed by Hong et al. [52] on the assembly of charged Janus spheres showed that the charge asymmetry of a single JP is preserved in the cluster acting as a larger charged JP.

From theoretical calculations, an amphiphilic JP, half hydrophobic and half hydrophilic, can be up to three times more active at the interface than the corresponding HP [31]. In these energetic calculations, the JPs are not aggregated, which is rather difficult to achieve experimentally if the particles exhibit a strong wettability contrast between both hemispheres. One way to avoid the aggregation of the JPs is to functionalize the particle surface with hydrophobic and hydrophilic ligands [27,43]. The electrical charge of the hydrophilic ligand plays a decisive role in the stabilization of JPs and the hydrocarbon chain of the hydrophobic ligand also introduces a steric effect between particles. A combination of both effects is expected to stabilize metallic particles through an electrosteric mechanism [27,43]. As reported by Garbin et al. [44], capping ligands play a prominent role in determining both interparticle interactions and the particle-fluid interactions. The simplest model to describe the interfacial arrangement of particles is the hard disk model in which the particles are represented by hard entities placed at the interface. These particles do not interact when there is enough room for every nanoparticle, but they become close-packed when the area per particle is sufficiently low [53]. However, when the particles are functionalized with large polymers, Monte Carlo simulations and experimental data show a complex behavior compared to hard objects at liquid/liquid interfaces [54].

The direct deposition of the nanoparticles dispersed in a spreading solvent at the interface requires lower amount of nanoparticles than adsorption from the bulk. From the growing and shrinking of the pendant drop the interfacial activity of the nanoparticles can be evaluated and compared within a wide range of area per particle. Glaser et al. [28] observed that the self-assembly of JPs at the water-

hexane interface resulted in a significant decrease in the interfacial tension. Furthermore, they demonstrated an adequate control over the interfacial activity by tuning the particles' amphiphilicity via ligand exchange reactions. Liu et al. [55] simulated JPs with capping ligands of different length confined in a fluid-fluid interface and stretched the available area. The nanoparticle arrangement exhibited a reversible transition between random and long-ranged configurations that could be effectively controlled by various structural parameters of the Janus morphology and the applied pressure. They revealed that conformational entropy effect of the capping ligands and capping ligand differences dominated the collective nanoparticle organization in the mechanical response.

2. Adsorption of Janus particles at fluid-fluid interfaces: Theoretical aspects.

Janus particlesin particle-laden interfacesare being extensively studied due to their promising properties for applications in biotechnology, nanotechnology, electronics, and clean energy [56]. Particles larger than a few nanometers can be permanently attached to interfaces (e.g. water/oil) as the interfacial tension and the contact angle, which can result in large adsorption energy, E_{ads}:

$$E_{ads} = \pi r^2 \gamma_{12} (1 \pm \cos\theta_{12})^2 \quad (1)$$

where r is the particle radius, γ_{12} is the interfacial tension between the fluids and θ_{12} is the three-phase contact angle. It should be noted that the interfacial tension (γ_{12}) between both fluids strictly exists only when the particle size is small (smaller than 100 nm). For larger particle sizes, however, three phases are present and the interfacial tension is not defined. In this case, what is rigorously defined is the change of interfacial Gibbs energy, and it should be referred to as apparent interfacial tension. The sign $\pm$ inside the bracket is negative for removal from the water phase, and positive for removal from the air or oil phase. To get an idea about the order of magnitude of the adsorption energy, we assume a HP of r = 10^{-8} m adsorbed at the water/toluene interface (γ_{12} = 0.036 N/m) with θ_{12} = 90° and according to Eq. 1, E_{ads} is 2750 k_BT [23]. Above or below 90°, E_{ads} decreases rapidly such that for θ_{12} between 0° and 20° or between 160° and 180° this energy is relatively small (< 10 k_BT). One consequence of the very high energy of adsorption of particles with θ_{12} = 90°, relative to the thermal energy, is that these particles once placed at the interface are effectively irreversibly adsorbed. Therefore, we can say that colloidal particles spontaneously adsorbed at the interface between two immiscible fluids to minimize the interfacial area between the two phases. Nevertheless, the shape and wettability of particles have a strong influence on their configuration and interactions at fluid-fluid interfaces. For that reason, we will consider in this review both aspects: particle shape and wettability.

Binks and Fletcher [31] performed a theoretical comparison between the desorption energy of

spheres of uniform wettability (HPs) and JPs adsorbed at an oil-water interface as the amphiphilicity is tuned from zero to the maximum value. In comparing the adsorption of HPs and JPs, it is useful to distinguish between surface activity and amphiphilicity. A surface-active particle shows a tendency to adsorb at interfaces, whereas an amphiphilic particle possesses a diblock structure in which the two domains have different affinities for each fluid phase. HPs for which the contact angle at the oil-water interface is around 90° are strongly surface active although they are not amphiphilic. Instead, JPs are both surface active and amphiphilic [31]. The amphiphilicity of JPs can be tuned through variation of both the angle α (parametrizing the relative areas of the polar and apolar domains, see Fig. 1) and the magnitude of the difference between θ_A and θ_P, the equilibrium contact angles of the two domains of the particle adsorbed at the oil-water interface. Zero amphiphilicity (corresponding to HPs) corresponds to either α = 0°/180° or (θ_A-θ_P)= 0°. The strongest amphiphilicity is expected when α = 90° and $|\theta_A - \theta_P|$ = 180°. The total surface free energy E of a JP at an oil-water interface as a function of the angle β (characterizing the immersion depth of the particles, see Fig. 1) are given by:

For $\beta \leq \alpha$

$$E(\beta) = 2\pi r^2 \left[\gamma_{AO}\,(1+\cos\alpha) + \gamma_{PO}(cos\beta - cos\alpha) + \gamma_{PW}(1-cos\beta) - \frac{1}{2}\gamma_{OW}(sin^2\beta)\right] \quad (2)$$

and for $\beta \geq \alpha$

$$E(\beta) = 2\pi r^2 \left[\gamma_{AO}\,(1+\cos\beta) + \gamma_{AW}(cos\alpha - cos\beta) + \gamma_{PW}(1-cos\alpha) - \frac{1}{2}\gamma_{OW}(sin^2\beta)\right] \quad (3)$$

where r is the particle radius and γ_{AO}, γ_{PO}, γ_{AW}, γ_{PW} and γ_{OW} are the interfacial tensions of the apolar-oil, polar-oil, apolar-water, polar-water, and oil-water interfaces, respectively. Eqs. 2 and 3 are valid under conditions such that the radius of curvature of the oil-water interface is negligible relative to the particle radius and are applicable to the case in which micrometer-sized liquid drops are coated with nanometer-sized particles. For the case of nanoparticles considered by Binks and Fletcher [31] where their density is not too different to that of the bulk oil and water phases, the oil-water interface shape is not significantly deformed by particle buoyancy effects. It is further assumed that the JPs are oriented with the apolar region all or mostly in the oil phase and the polar region all or mostly in the water. In addition, effects of the line tension associated with the liquid-solid perimeter line around the particle were neglected. The desorption energies for different particle radii and interfacial tension scale as the product $\gamma_{OW} \cdot r^2$.

The contact angles θ_A and θ_P correspond to the equilibrium angles given by the Young's equation as follows:

$$cos\theta_A = \frac{\gamma_{AW} - \gamma_{AO}}{\gamma_{OW}} \quad (4)$$

$$cos\theta_P = \frac{\gamma_{PW} - \gamma_{PO}}{\gamma_{OW}} \quad (5)$$

The average contact angle of the JP is weighted by the relative areas of the polar and apolar domains as follows:

$$\theta_{average} = \frac{\theta_A(1+cos\alpha) + \theta_P(1-\cos\alpha)}{2} \quad (6)$$

The immersion angle β corresponding to the minimum surface energy configuration of the JPs depends on the relative magnitudes of α, θ_A and θ_P. The three possibilities are listed here:

$$\begin{aligned} &\text{For } \alpha<\theta_A<\theta_P, \text{ then } \beta=\theta_A \\ &\text{For } \theta_A<\alpha<\theta_P, \text{ then } \beta=\alpha \\ &\text{For } \theta_A<\theta_P<\alpha, \text{ then } \beta=\theta_P \end{aligned} \quad (7)$$

Eqs. 2 and 3 together with the inequalities in Eq. 7 allow the calculation of the minimum surface energy of the adsorbed particle, E_{ads}. The surface energy of the particle located entirely in either the bulk oil (E_{oil}) or water (E_{water}) is given by Eqs. 2 and 3 with β set to either 0° (for the particle in oil) or 180° (for the particle in water). The surface activity of the particle was calculated by Binks and Fletcher [31] as the desorption energy, which is defined as the free energy required to desorb the particle from the interface into either the bulk oil or water phase, (E_{oil}-E_{ads}) or (E_{water}-E_{ads}), whichever is the lowest.

Fig. 2 shows the variation of particle desorption energy in units of k_BT per particle for different values of the angle Δθ (defined as $|\theta_A - \theta_P|/2$). For this series, α, r, and γ_{OW} were set to constant values of 90°, 10 nm, and 36 mNm^{-1}, respectively. According to the different selected contact angles, the appropriate combinations of surface energies were obtained by solution of Eqs. 4 and 5.

For this series at constant α, the particle amphiphilicity is tuned by changing Δθ. The case Δθ = 0° corresponds to a HP with zero amphiphilicity, Δθ = 90° corresponds to the maximum possible amphiphilicity in which the polar region of the particle is completely wetted by water and the apolar region is completely wetted by oil.

As can be seen in Fig. 2, as increasing the particle amphiphilicity through Δθ, the strength of particle adsorption increases up to a maximum of 3-fold for $\theta_{average}$ of 90°. In addition, the JPs maintain strong adsorption with average contact angles near 0° or 180°, where the surface activity of the HPs is low.

The most important conclusions that may be drawn of the study made by Binks and Fletcher [31] are: first, desorption energies may be increased 3-fold by maximizing the amphiphilicity of JPs; second, unlike HPs, JPs retain their strong adsorption even for average contact angles of 0° and 180°.

In relation to the stability of symmetric JPs (where the two different surface domains are of equal area) at fluid-fluid interfaces, Cheung and Bonn [57] demonstrated using Monte Carlo simulations that the presence of the particle at the interface became more stable as increasing the difference in affinity of the two faces with the respective liquid phase.

Hirose et al. [32] investigated the effect of the interface curvature on the JP adsorption and showed that although the equilibrium contact angle is determined by the classical Young's equation (being independent of the curvature), the adsorption energy is affected by the interfacial curvature. Fig. 3 shows the dimensionless adsorption energy ($g_i(\theta,\varepsilon)$, in Eq. 8) as a function of the contact angle θ and ε = r/R (r and R are the JP and the liquid drop radii, respectively), for a flat interface (ε=0) and two curved interfaces (ε = 0.2 and 0.4).

$$g_i(\theta,\epsilon) = \frac{w_i}{2\pi r^2 \gamma_{12}} - \gamma - \tau cos\alpha - \frac{r(p_1+p_2)}{3\gamma_{12}} \quad (8)$$

If the JP is divided into two parts as an angle α: A (hydrophilic) and B (hydrophobic), w_i (i= A,B) is the corresponding interfacial energy, 1 and 2 are the two fluid phases of the interface, γ_{12} is the interfacial tension between both fluids, $\gamma = \frac{\gamma_{1A}+\gamma_{2B}}{\gamma_{12}}$, $\tau = \frac{\gamma_{1A}-\gamma_{2B}}{\gamma_{12}}$, p_1 and p_2 are the pressures in each fluid.

Recently, the chance of to stabilize thermodynamically Pickering emulsions using JPs has been theoretically addressed by Aveyard [58]. The key-point is how the magnitude of the adsorption free energy of JPs can affect the emulsion formation with negative changes in its free energy. In the lateral interactions between particles adsorbed at drop surfaces the electrical, hydration and van der Waals forces were taken into account. Following a simple approach, Aveyard showed that emulsions stabilized by JPs are thermodynamically stable because the large adsorption energy of these particles can overcome the free energy increase for the formation of a bare oil-water interface. Furthermore, Aveyard found that the long-range electrostatic repulsion can play a prominent role in the stabilization of Pickering emulsions with JPs and the van der Waals attraction appears to be negligible in all cases. A theoretical study performed by Tu et al. [59] confirmed that the Pickering emulsions can be stabilized by using amphiphilic Janus dumbbells, which are nonspherical particles made of two partially fused spherical particles of opposite wettability. To the best of our knowledge, there is not yet experimental evidence of these theoretical predictions.

Recently, there is a growing interest in the study of non-spherical JPs and particularly in ellipsoidal particles with different aspect ratio adsorbed at liquid-liquid interfaces [49,60-63]. This type of JP has an additional degree of freedom in tuning the particle characteristics, for example, Janus paramagnetic ellipsoids have been shown to exhibit unique response to a rotating magnetic field [64]. Park and Lee [60] theoretically studied the equilibrium orientation of nonspherical JPs adsorbed at an oil-water interface. The equilibrium orientation of a Janus nanoparticle at this interface is the result of

two competing driving forces: (1) the minimization of the unfavourable water-oil interactions, which is obtained when the Janus nanoparticle occupies as much interfacial area as possible, and (2) the minimization of Janus nanoparticle-solvent interactions, which is obtained when the polar beads on the Janus nanoparticle interact preferentially with water beads. Two types of particles were considered: Janus ellipsoids and Janus dumbbells. The equilibrium orientation was calculated on the basis of a minimum condition in the adsorption energy as a function of the orientation angle respect to the oil-water interface. In general, it was found that this type of JPs adopts the upright orientation (i.e., the major axis of the ellipsoid or dumbbell is perpendicular to the interface) if the difference in the wettability of the two regions is large or if the particle aspect ratio is close to 1. Otherwise, the nonspherical JPs would tend to have a tilted orientation at equilibrium. Another important conclusion of this theoretical study is that the interaction potential between Janus dumbbells showed only a primary energy minimum indicating that these particles prefer always to be in a single orientation, whereas Janus ellipsoids, under appropriate conditions, can be kinetically trapped in a metastable state due to the presence of a secondary energy minimum. In consequence, as Park and Lee affirm, the orientation of nonspherical JPs likely will have important influence on their ability to stabilize emulsions and modify the rheological properties of fluid interfaces. Whereas Park and Lee [60] found theoretically that in some cases it is possible thatan ellipsoidal JP at a liquid-liquid interface adopts two well-defined orientations (one is representative of the equilibrium orientation, while the second one represents a local minimum in the free-energy landscape), Luu et al. [61] using dissipative particle dynamics simulations found that the ellipsoidal JP has one preferential orientation although they oscillate around it. The same conclusion was reached when the ellipsoidal JPs were assembled at spherical oil-water interfaces [63]. It is possible that the temperature of simulated systems provide sufficient fluctuations that the JPs escape the local minima discussed by Park and Lee [60]. Concerning to interfacial tension, Luu et al. [61] found that the ellipsoidal JPs reduce the decane-water interfacial tension more efficiently than spherical ones, provided that the nanoparticle surface density is high. For a given nanoparticle shape, the interfacial tension reduction becomes more significant as the percent of nonpolar beads on the nanoparticle surface increases. Analysis of simulation results suggested that prolate and oblate nanoparticles are more effective than spherical particles in reducing the interfacial tension because of the larger excluded volume, which increases when the nanoparticle orient their longer axis parallel to the interface. These results are consistent with experimental data obtained by Ruhland et al. [34] with Janus cylinder.

Although in literature there is none comparative study of the self-assembly and rheological behavior between ellipsoidal Janus and homogeneous particles, there are good experimental data with ellipsoidal homogeneous particles [65-67]. However, theoretically we know that in the study of the interactions of ellipsoidal JPs at an oil-water interface unlike homogeneous ellipsoids with quadrupolar deformations, Janus ellipsoids induce a hexapolar interface shape due to the change in

meniscus sign by crossing the Janus boundary. The overlapping of such distortions for neighboring particles leads to long-ranged capillary interactions [62].

Gao et al. [68] have also studied using molecular dynamics simulations the influence of shape of JPs on their orientation and interface activity at fluid-fluid interfaces. Three types of JPs were considered: spheres, rods and discs. In the simulations, Gao et al. considered four types of beads: JPs constructed by lumping Lennard-Jones (LJ) beads with different types at one of the two halves of the JP surface. Two "atomic" types of LJ beads modelled the immiscible fluids.

The beads interacted with each other through a shifted-force Lennard-Jones potential. A linear term was added so that the force smoothly went to zero at cut-offdistance in Eqs. 9 and 10.

$$U(r_{ij}) = \begin{cases} 4\varepsilon\left[\left(\frac{\sigma}{r_{ij}}\right)^{12} - \alpha_{ij}\left(\frac{\sigma}{r_{ij}}\right)^{6}\right] + \Delta U(r_{ij}) & r_{ij} < r_c \\ 0 & r_{ij} \geq r_c \end{cases} \quad (9)$$

and

$$\Delta U = -(r_{ij} - r_c)\frac{\partial U_{LJ}}{\partial r_{ij}}(r_c) \quad (10)$$

Here, r_{ij} is the distance between two beads, σ is the bead size, ε is the interaction potential well depth, and the potential is cut-off at $r_c = 2.5\ \sigma$. For simplicity, all the beads in the system had the same size σ and mass m. The symmetric coefficient matrix $\alpha_{ij} = \alpha_{ji}$ $(0 \leq \alpha \leq 1)$ controls the attraction between beads of different types in the simulations, which in turn determined the wetting properties.

The free energy profiles for the different morphologies Janus spheres, Janus rods and Janus discs transferring from a fluid phase to the interface are shown in Fig. 4. In this scheme, θ_{int} corresponds to the initial orientation angle between the JP and the planar interface and $\beta = \alpha_0 - \alpha_1$ $(0 \leq \beta \leq 1)$ the index of amphiphilicity, being α_0 and α_1 a measure of the surface wettability of the JP by the two fluids. For Janus spheres and rods, they had a free energy minimum at the interface, irrespective of the initial orientation of the JPs. Therefore, there is one equilibrium orientation for both Janus spheres and Janus rods at the fluid-fluid interface. In comparison, upon contact to the interface, Janus discs with different initial orientation angles follow different pathways ending up in two different final orientations, corresponding to forward orientation and reverse orientation, respectively. The existence of two different orientations of the Janus discs at the fluid-fluid interface indicates that some Janus discs can be kinetically trapped in a metastable orientation, and the initial orientations of Janus discs have a great impact on their final orientation. Apparently, Janus discs are the most efficient to stabilize a fluid interface. But this interface may be metastable depending on the orientation of the Janus discs at the interface.

The fluid-fluid interfacial tension, γ, was calculated from the difference in the diagonal components of

the pressure tensor (a planar interface was assumed in the simulations) averaged over the entire interface as follows:

$$\gamma = \frac{1}{2}\langle L_z \left(P_{zz} - \frac{P_{xx}+P_{yy}}{2} \right) \rangle \quad (11)$$

Where L_z is the box length in z direction (i.e. , normal to the planar interface), and P_{ii} is the diagonal component of the viral tensor (i = x, y or z). Fig. 5 shows the time evolution of interfacial tension of fluid-fluid interface by adsorbing, respectively, Janus spheres, Janus rods, and Janus discs with different β at a particle volume fraction of 0.13. The interfacial tension showed a rapid decrease at early stages of adsorption for all types of JPs, which levelled off and reached a stable value. A change in shape of the JPs led to different adsorption behavior at the interface. As can be seen in Fig. 5, Janus spheres are not so efficient to decrease the interfacial tension; in contrast Janus rods most efficiently reduced the interfacial tension. Janus discs with smaller values of β showed similar efficiency on interfacial tension reduction, but increasing β will decrease the ability of Janus discs to reduce the interfacial tension. These results clearly demonstrated that anisotropy in the shape of JPs, as earlier indicated by Park and Lee [60], leads to a decisive influence on the surface activity. It should be noted that for Janus spheres and Janus rods the interfacial tension reduction was independent on β, while for Janus discs the interfacial tension reduction became more significant as β decreased. These simulated results of interfacial tension are in a reasonable agreement with the experimental data of interface activity measured by Ruhland et al. [35] with JPs of similar geometries to those used by Gao et al. [68].

3. Surface activity and interfacial behavior of Janus particles adsorbed at fluid-fluid interfaces: Experimental data

3.1 Experimental studies performed using a Langmuir balance.

The Langmuir film balance technique is very used to characterize the interfacial activity and arrangement of nanoparticles at water/air and water/oil particle-laden interfaces [27,43,69,70-71].

To best of our knowledge, Sashuk et al. [43] were the first ones to experimentally study the surface activity of Janus-type nanoparticles at the water/air interface using a Langmuir balance. The aim of this study, however, was to develop a simple method to obtain close-packed and charged colloidal monolayers of well-defined surface charge at the air-water interface, which can be easily transferred onto solid substrates. This method is based on the fact that ligands forming the protecting layer around noble metal nanoparticles exhibit ability to arrange at the nanoparticles surface [72-73]. Sashuk et al. demonstrated that if the protecting layer is composed of a mixture of hydrophobic (1-undecanthiol (UDT)) and hydrophilic charged ligands (11-mercaptoundecanoic acid (MUA) and

N,N,N-trimethyl (11-mercaptoundecyl) ammonium chloride (TMA), for the negatively silver and positively gold charged nanoparticles, respectively) in appropriate proportions (10-15% of the hydrophilic ligand), the nanoparticle becomes Janus-like with a contrast of wettability between both hemispheres of the particle. The surface pressure-area (Π-A, where $\Pi = \gamma_0 - \gamma$, with γ_0 the surface tension without JPs and γ the measured surface tension with JPs) isotherm recorded by Sashuk et al. for the colloidal monolayer composed of positively charged gold containing 10% of TMA in the protecting layer (10Au+) is shown in Fig. 6. As can be seen in this figure, the compression proceeded without any noticeable change in Π down to ≈200 nm^2/nanoparticle. Below this point (the gas-liquid transition), a steep rise in the surface pressure was observed. The threshold value of about 200 nm^2/nanoparticle corresponds to the average surface-surface distance between the nanoparticles of about 3 nm, which can serve as a rough estimate of the Debye screening length in the aqueous phase. The presence of electric charge allowed compressing the colloidal monolayer up to a relatively high surface pressure of about 40 mN/m. Further compression resulted in the collapse of the colloidal monolayer. At the collapse point, the area occupied by a single nanoparticle was about 100 nm^2, which is very close to the value found for a hexagonally close-packed monolayer, 117.5 nm^2/nanoparticle assuming a radius of 5.42 nm per particle.

The hysteresis displayed by the Π-A isotherm in Fig. 6 was mostly due to migration of a small fraction of 10Au+ nanoparticles into the aqueous phase. From thermodynamics point of view, the existence of hysteresis cycles is always interpreted as an experimental evidence of lack of equilibrium.

The contact angles of both hemispheres were (91.5±2)° and (80.5±1.5)°, which proved that the two hemispheres of the nanoparticles presented different hydrophilicity. Also, data obtained with FITR spectroscopy suggested that the Janus structure was formed during the ligand exchange process but the ligands only rearranged when the nanoparticles were brought at the water/air interface.

Recently, Reguera et al. [37] have presented an experimental approach based on Neutron Reflectivity (NR) that allows in-situ measurements of the contact angles of nanoparticles (NPs) adsorbed at fluid interfaces. They used two sets of gold nanoparticles, one coated by a single ligand, perdeuterated 1-octanethiol (d-OT) and the other one coated by two ligands, perdeuterated 1-octanethiol and 6-mercapto-1-hexanol (d-OT:MHol 1:1). In the first set of NPs, the experimental value of contact angle was 119.5 ± 5.5°, which was in good agreement with 121° determined from simulation. Concerning to the d-OT:MHol 1:1 sample of NPs, the value of contact angle was 85 ± 10°, which is much lower than that of d-OT NPs as expected due to the presence of hydrophilic ligands. The most important conclusion of this comprehensive study on the contact angle measurement is that the Janus structure was not present in their NPs because the ligands were uniformly distributed on the gold surface, suggesting that the capping ligands did not rearrange in Janus-like form when the NPs were placed at the interface. This would imply that the *one-pot* method might be in fact a wrong strategy for

synthesis of JPs. Nevertheless, nanoparticles synthesised by one-pot method and that involves the sequential functionalization of the particle surface with thiol-terminated polyethylene glycol (PEG) chains and short alkane-thiol molecules have demonstrated to be highly effective emulsifying agents. This emulsification effect is due to the strong adsorption of this type of particles at oil-water and air-water interfaces, although they must not be considered as JPs [36].

3.2 Experimental studies performed using pendant drop tensiometry.

Pendant drop tensiometry is an extensively employed method for measuring surface and interfacial tension of liquids [74]. The surface tension of JPs can be measured using pendant drop tensiometry. As Ruhland et al. [34] state, an elegant way of determining the influence of particles at liquid-liquid interfaces is to analyze the interfacial tension of a dispersion of the desired material via the pendant drop method. This technique enables to measure the surface or interfacial tension of colloidal monolayers using a much smaller amount of particles than that the well-established technique of Langmuir balance, where the particles are spread on a fluid subphase from a volatile solvent to form the monolayer [44]. Instead, the colloidal monolayer is formed onto the surface of a pendant drop with a few microliters of solution. This is very important because for the JPs synthesis simple strategies are still being developed for the preparation of large amounts of JPs [24].

A typical set-up is composed of a CMOS camera interfaced with a computer-based data acquisition system, which is used to capture the image of an equilibrium drop [75]. Then edge-detecting software is used to fit the drop shape to the Young-Laplace equation using the Axisymmetric Drop Shape Analysis Profile (ADSA-P) [74]. Real time drop images are processed at each step of volume variation and the drop area and surface tension are calculated [74]. It is strongly required for the reference system of two fluids that the drop phase and the particle solution are immiscible. An initially relatively high interfacial tension is additionally beneficial to produce a large driving force for the JPs to assemble at the interface. Furthermore, the density of the liquid forming the drop needs to be higher than the surrounding dispersion liquid in order to ensure the development of a hanging drop at the end of the syringe needle. To the best of our knowledge, Kwok et al. [76] were the first in using the axisymmetric drop shape analysis (ADSA) as a film balance. They studied the surface behavior of an octadecanol monolayer.

Although the quantity of nanoparticles required is much lower than that necessary for a standard Langmuir film balance experiment, a certain amount of nanoparticles is still necessary for the experiments that involve the adsorption of JPs at the interface of a pendant drop from the bulk [25,34,42,77]. When the sample amount is insufficient to study the adsorption from the bulk to the interface of the pendant drop, the direct deposition of the nanoparticles onto the drop interface from a volatile solvent allows the study of the interfacial activity. Moreover, solvent evaporation is a violent and rapid process, which helps the nanoparticles to be adsorbed at the interface of the pendant drop,

faster than the diffusion from the bulk [44]. This methodology enables to control the amount of nanoparticles deposited at the interface, contrary to the diffusion from bulk experiments in which the control parameter is the initial concentration of particles in the bulk. Nevertheless, neither method presents the possibility to know a priori the exact amount or microstructure of the particles that finally are placed onto the interface.

a) Water/hexane.

Glaser et al. [28] were the first in presenting experiments on the interfacial activity of JPs (gold and an iron oxide moiety) at fluid-fluid interfaces, where the JPs were diffusing from the hexane phase onto the water pendant drop interface.The aim of this study was to provide an experimental confirmation of Binks' theoretical prediction whereby the stabilization of Pickering emulsions should be considerably improved when JPs instead of HPs are used [31]. The JPs were made of an Au and Fe_3O_4 part following the protocol of Yu et al. [78]. The mean diameter of the gold particle was around 4 nm and the diameter of iron oxide was about 10 nm, resulting in an overall diameter of about 14 nm.

To establish the effect of the Janus character of the particles on their interfacial activity, HPs of both gold and iron oxide of comparable sizes were synthesized as well, 10 and 7 nm in diameter, respectively. Oleic acid and oleylamine were used as ligands for the homogeneous iron oxide nanoparticle as well as the iron oxide part of the JPs. To increase the amphiphilic character of the JPs further, dodecanethiol (DDT) and octadecanethiol (ODT) molecules were attached to the gold part via ligand exchange. The excess thiol and ligands at the iron oxide part were properly removed. This cleaning process is crucial to obtain meaningful values of interfacial tension using pendant drop tensiometry because the desorption of any ligand from the JP greatly can affect to the interfacial tension. For quantitative comparison, the homogeneous gold nanoparticles were also capped with DDT following the same procedure as for the JPs.

The concentration of nanoparticles in solution was about $1.2 \cdot 10^{-4}$ mmol/L (i.e., $7 \cdot 10^{16}$ nanoparticles/L). As can be seen in Fig. 7, as soon as the water drop is formed, the water/n-hexane interfacial tension begins to decrease as the particles adsorb at the interface. For the homogeneous particles, similar values of the interfacial tension were found after 1000 s (Fe_3O_4: 34.5 mN/m; Au: 33 mN/m). These values were lower than for the water/hexane interface, which was around 48 mN/m in the absence of surface-active agents.

For the JPs modified with DDT (JP_{DDT}) the interfacial tension dropped up to 22.5 mN/m. This decrease in the interfacial tension of the JPs in comparison with the HPs confirmed that the JPs are considerably more effective to reduce the interfacial tension as expected and according to the Binks' theoretical prediction [31]. It can be concluded that the JPs orient at the liquid-liquid interface. Because of its nonpolar character, the hydrocarbon ligand-covered gold part should point to the hexane phase, and the polar iron oxide should be (partially) immersed in the water phase (see scheme

in Fig. 8). If ODT ($C_{18}H_{37}SH$) replaces DDT ($C_{12}H_{25}SH$) then the interfacial tension reached a minimum value of 18 mN/m. Obviously, the particle concentration of JP_{DDT} in hexane plays an important role in the decreasing of the interfacial tension and the lowest value of the interfacial tension measured was around 12 mN/m at a JP_{DDT} concentration of $3.9 \cdot 10^{-4}$ mmol/L. This value of concentration is approximately 4 orders of magnitude lower than for typical surfactant, e.g., AOT. This reveals the significant advantages of JPs in the stabilization of emulsions and foam.

b) Perfluorinated oil-dioxane and perfluorinated oil-dimethyl sulfoxide interfaces.

Ruhland et al. [34] were the pioneers in the study of the self-assembly of Janus cylinders at liquid-liquid interfaces. The Janus cylinders were characterized by a phase separation along the major axis into two hemicylinders of different wettability. They used the pendant drop tensiometry and microscopic imaging to characterize the adsorption behavior and self-assembly of Janus cylinders at perfluorinated oil-dioxane and perfluorinated oil-dimethyl sulfoxide interfaces. The key difference between spherical and anisotropic particles is the number of transitions in interfacial tension that can be encountered during concentration changes.

The synthetic pathway to obtain cylindrical Janus structures was based on a template-assisted synthesis, involving cross-linking of a microphase-segregated lamellar-cylinder morphology of a bulk film of polystyrene-block-polybutadiene-block-poly-(methyl methacrylate) (SBM) block terpolymer, followed by a sonication treatment. This process resulted in the formation of core-crosslinked cylinders, possessing a polybutadiene (PB) core and two hemicylinders of PS and PMMA. The PB cylinder had an average diameter of approximately 23 nm with a surrounding corona, leading to a total diameter of the cross section of 80 nm. They chose perfluorooctane (PFO) as the drop phase and dimethyl sulfoxide (DMSO) and dioxane as solvents in order to get sufficiently high interfacial tensions with values of 21.7 (PFO/DMSO) and 10.7 mN/m (PFO/dioxane), respectively.

In a first series of experiments, they assessed the influence of different length of the Janus cylinder on the interfacial tension of liquid-liquid interfaces for the two systems. Fig. 9 displays a series of pendant drop tensiometer measurements for cylinders with number of average lengths of 2300, 1600, 800 and 350 nm, dissolved in dioxane at a concentration of 1 g/L. As can be seen in Fig. 9, the interfacial tension decreased with time and approached quasi-equilibrium. At early stages of adsorption, the interfacial tension decreased rapidly. Subsequently, the decrease in interfacial tension slowed down, and finally, it approached a plateau, where the maximum coverage of the interface with cylinders was obtained. After reaching the plateau value, the Janus cylinders were located and arranged at the interface. An increase of the average length of the Janus cylinders led to an enhanced adsorption at the interface, and the plateau was reached earlier. The differences observed in Fig. 9c are probably due to the lower viscosity of dioxane (1.37 mPa.s) compared to DMSO (2.24 mPa.s), which affects obviously to the diffusion coefficients and the adsorption kinetics of cylinders onto

liquid interfaces.

Presumably, the Janus cylinders are orientated parallel to the liquid-liquid interface and their interfacial assembly is evidently determined by a minimization of the free energy. Hence, the longest Janus cylinders had most influence on the interfacial tension and the highest surface activity (see Fig. 9). Considering the values of solubility parameters of the various polymers, it has sense to assume that PS is preferably orientated towards the PFO phase and the PMMA side chains towards the external solute phase (dioxane or DMSO). If we compare the interfacial tension isotherms of the uncrosslinked polymer (SBM) and the Janus cylinders (see Fig. 9), we can conclude that the block terpolymer provides a minor reduction of around 10% of the interfacial tension for both solvents, however, the Janus cylinders showed a significantly stronger decrease, i.e., an up to 5-fold better performance for the PFO-dioxane solvent system and up to 4-fold better performance for PFO-DMSO. These results indicate that Janus cylinders are more efficient stabilizing agents for the nanostructuration of interfaces than the block terpolymers.

Concerning to the mechanism of cylinder adsorption, Ruhland et al. [34] found that the adsorption took place following three different stages (see Fig. 10). First, there was free cylinder diffusion to the interface (I). Therefore, the number of particles at the interface increased rapidly, the cylinders packed closer, and the decrease in interfacial tension slowed down (II). Furthermore, similar to phase II a closer cylinder organization played an important role in order to get more cylinders to the interface (III). Here, the adsorption of new Janus cylinders came along with a rearrangement and better ordering of already adsorbed cylinders at the interface. These microscopic arrangements of the Janus cylinders at the interface were confirmed by ex-situ TEM images (see Fig. 10).

c) Toluene-water interface.

Recently, Ruhland et al. [35] have again studied the influence of JP shape (spheres, cylinders and discs) on their interfacial behavior at liquid-liquid interfaces, but now using the toluene-water interface. As previously, the synthetic pathway to obtain JPs was based on a template-assisted synthesis, involving cross-linking of a bulk terpolymers and a subsequent sonication treatment. The block terpolymer precursors used in the preparation of cylinders and spheres JPs were: the two polystyrene-block-polybutadiene–block-poly(methyl methacrylate) block terpolymers $S_{41}B_{41}M_{45}$ and $S_{44}B_{8}M_{48}$, respectively. Whereas, the polystyrene-block-polybutadiene-block-poly(tert-butyl acrylate) block terpolymer $S_{42}B_{10}T_{48}$ was the block terpolymer precursor of the Janus discs. The geometries of JPs synthesized by Ruhland et al. [35] are shown in Fig. 11.

Pendant drop tensiometry isotherms of the interfacial tension at the toluene/water interface (γ = 34 mN/m) were measured on a Krüss DSA100 tensiometer at room temperature. The measurements were performed with a degassed Milli-Q-water droplet saturated with toluene immersed in a toluene solution of the JPs saturated with water. The interfacial tension was measured as a function of time

(see Fig. 12). Different adsorption dynamics for spheres, cylinders, and discs were observed. The addition of Janus cylinder resulted in the maximum reduction in the equilibrium interfacial tension, from 34 to ca. 14 mN/m. In comparison, Janus spheres showed a moderately lower surface activity with an intermediate γ_∞ value of ca. 17.5 mN/m. Janus discs provided the smallest amount of effective interfacial tension reduction, from 34 to ca. 19 mN/m. Additionally, the Janus discs showed a different trend of adsorption dynamics, which clearly pointed toward a change in the packing of the Janus discs at the interface with time due to the anisotropic shape.

As pointed out by the authors of this very interesting comparative study on the self-assembly behavior of JPs with different geometries at the toluene/water interface, one reason for the different adsorption kinetics is the size of the JPs. The Janus spheres were 50 nm in diameter, whereas the cylinders had a length of 2300 nm and the discs were around 300 nm. Smaller sizes led to higher diffusion coefficients and thus faster adsorption kinetics, however, the particle shape is also a determining factor of the quasi-equilibrium state and the final value of the interfacial tension. The ability for stabilization slightly decreases from Janus cylinders to Janus spheres to Janus discs. Ruhland et al. [35] simulated the free energy change upon adsorption of the various types of JPs to get a better understanding of the adsorption behavior and kinetics of JPs at liquid-liquid interfaces. The free energy of adsorption for the particles at the interface was calculated similarly to the method used by Pieranski [79] at a series of rotations and translations through the interface from the Eq. 12.

$$\Delta G_{ad} = \sum_P A_{P1}\gamma_{P1} + \sum_P A_{P2}\gamma_{P2} - A_{12}\gamma_{12} \quad (12)$$

Where A_{ij} represents the area and γ_{ij} the interfacial tension with the subscripts P1, P2 and 12 for the polymer phase in liquid 1, the polymer phase in liquid 2, and the fluid-fluid interface, respectively. The values of the areas were calculated by simply summing the area of triangles of the PMMA or PS phase in the corresponding liquid phase. The interfacial tension values used in the calculations were: water-toluene, 34 mN/m; PS-toluene, 6.5 mN/m; PS-water, 32 mN/m; PMMA-toluene, 11.4 mN/m; PMMA-water 16 mN/m. The simulation method was the same used by Morgan et al. [80] to evaluate the adsorption energy of hematite particles at a liquid interface. On the basis of calculated data, these authors found a favoured orientation of PS to the toluene phase and PMMA side chains to the water phase. The energy barrier for the removal an isolated Janus sphere from the interface is $\approx 5{\cdot}10^5\,k_BT$. In comparison, the energy profile of Janus discs showed two energy minima and therefore predicted the existence of two different orientations, which correspond to the global and local minimum energies, of the Janus discs at the toluene-water interface. The energy barriers were $\approx 1.5{\cdot}10^6\,k_BT$ and $5{\cdot}10^5\,k_BT$, respectively. The Janus cylinders had one energy global minimum of $1{\cdot}10^6\,k_BT$ with an orientation parallel to the interface. On the basis of the experimental data and simulation results, Ruhland et al.

[35] were able to describe the fundamental aspects of adsorption kinetics of the JPs at liquid-liquid interfaces, which depend not only of the particle size but also of the geometrical shape of particles. Whereas the adsorption kinetics of spheres and cylinders can be described by three different adsorption stages, the discs require of four stages (see Fig. 12).

d) Water/air and water/decane interfaces.

Park et al. [45] have studied the behavior of JPs (gold-coated polystyrene particles-AuPS) at an oil-water interface formed between decane (superphase) and an aqueous subphase with 2 %wt of Gellan (Gellan gum is a water-soluble anionic polysacchraride produced by the bacterium Sphingomonas elodea), JPs were inserted at the interface with a spreading solvent (isopropanol). The spreading agent plays a crucial role in the formation of well-structured colloidal monolayers, although the effects that cause on the colloidal stability of particles and the surface tension of the fluid-fluid interfaces are not very well understood yet [81]. To investigate the effect of the wettability of the gold hemisphere on the interfacial behavior of JP, the gold surface was modified using 1-dodecanethiol (DDT), 1-octadecanethiol (ODT) and 3-mercaptopropionic acid (MPA). The water contact angles of a water drop on a un-modified and thiol-modified gold (Au) were: Au (119±5)°, DDT-Au (139±3)°, ODT-Au (152±2)° and MPA-Au (62±2)°.

The behavior of the amphiphilic JPs at the decane-water interface was completely different from that of un-modified PS particles (PS, diameter 2.9 μm). Whereas the un-modified PS particles and MPA-Au-PS are organized into a stable hexagonal lattice, Au-PS JPs, ODT-Au-PS, and DDT-Au-PS immediately are aggregated giving rise to fractal structures. This observation suggested to Park et al. [45] that the formation of stable colloidal monolayers was the result of long-range electrostatic dipolar repulsions between the electrically charged particles [79] and that the attractive interaction associated with the uncharged JPs and the formation of fractal structures was due to capillary interactions provoked by an undulating contact line around the particle surface [82]. A simpler explanation could be that the weakly charged colloidal particles coagulate easily when they are placed at fluid interfaces [83]. Hong et al. have experimentally found the formation of clusters of charged Janus spheres [52]. The cluster shapes were analysed by combined epifluorescence microscopy and Monte Carlo computer simulations with excellent agreement. The most interesting result obtained in that work was that the charge asymmetry of individual JPs was preserved in the clusters. The low colloidal stability of the most JPs explains why the fluid-like, glass–like and hexagonal solid structures are not present at the JPs laden-interfaces, whereas these microstructures appear very often at the homogeneous particles laden-interfaces [84,85]. On the contrary, the amphiphilic JPs tend to form supermicelles because they behave like surfactants [46]. In this context, Beltran-Villegas et al. [50] have recently simulated using Brownian dynamics the equilibrium phase behavior of Janus colloids by implementing a sedimentation equilibrium approach, but the obtained information is not applicable to the possible

microstructures at JPs laden-interfaces. Furthermore, Tran et al. [86] recently found the coexistence of multiple stable mesophases for JPs based on lipids and stabilized by Pluronic F127 surfactant.

On the other hand, Fernandez-Rodriguez et al. have made a comparative study between gold and Janus gold particles behaviour at air-water and water-decane [87]. Homogeneous gold nanoparticles (AuC6) capped with hexanethiol (HPs) were synthesized following the Brust protocol [88]. Janus gold nanoparticles (JPs) were synthesized by functionalizing a hemisphere of the HPs with 2-(2-mercapto-ethoxy)ethanol (MEE) using the Chen protocol [27,71]. In some cases the hydrophilic MEE was substituted by the 3-mercaptopropane-1,2-diol (MPD). The terminal groups were -CH_3 and -*OH* for the hexanethiol and MEE or MPD functionalized hemispheres, respectively. Both nanoparticles were redispersed separately in tetrahydrofuran as a spreading agent (THF). The JPs diameter quantified from isolated nanoparticles in High Resolution TEM (HRTEM) pictures was (3.5±0.9) nm. The amphiphilic character of the Janus gold particles was examined by contact angle measurements. The hydrophobic side showed an average contact angle of (63.3±2.7)° (using MPD) or (56.1±1.8)° (using MEE), whereas it decreased up to (53.4±2.9)° (MPD) or (49.0±1.3)° (MEE) into the hydrophilic side. The wettability differences between -CH_3 and –OH terminal groups suggested a surface activity of the JPs. Atomic Force Microscopy (AFM) confirmed the amphiphilic nature of these Janus gold particles [89]. The mean value of the adhesion force between the Janus gold particles and a modified gold surface was found to be (31.5±10.0) nN, whereas this force diminished up to (27.5±4.5) nN when homogeneous (AuC6) particles were used. This latter value of adhesion force was very close to the mean value estimated for the direct contact between the AFM tip and the modified gold surface (C6 self-assembled monolayer surface). In any case, Perro et al. have pointed out that the direct visualization of the surface dis-symmetry of the JPs is not a simple task, as the difference between the two hemispheres is at the molecular level [21]. In addition to the AFM characterization of the structural details of the JPs, Nuclear Overhauser Enhancement Spectroscopy (NOESY) has also been used [71]. This is a two-dimensional phase-sensitive NMR technique that detects the distance-dependent nuclear Overhauser effect between proton spins. This spectroscopy technique also confirmed that the gold JPs prepared by Chen's method exhibited segregated distribution of the two kinds of ligands, supporting the amphiphilic structural model of these JPs prepared using the Langmuir-Blodgett technique. Nevertheless, it must be pointed out that because of the anisotropic characteristics and absence of electric charges on the JP surface, extensive aggregation was also observed in selected solvent media (THF) [87]. The low colloidal stability of these JPs is a serious drawback for a proper characterization of their interfacial behavior or surface activity.

Fernandez et al. [87] used the pendant drop tensiometry to precise change and control the volume and therefore the area of a MilliQ water pendant drop using a microinjector. The growing and shrinking of the pendant drop volume forced different nanoparticle arrangements, once a fixed amount of nanoparticles was adsorbed at the pendant drop interface. First, they deposited a given

amount of the HPs or JPs dispersed in THF onto a MilliQ water pendant drop in air with a microsyringe and a micropositioner and waited until full evaporation of the spreading solvent. As stated before, the evaporation of the spreading solvent ensured that the nanoparticles had enough energy to adsorb at the interface, compared with the slow process of adsorption from the bulk [44]. In Fig. 13, it can be observed the surface tension evolution over time after different amounts of HPs and JPs deposited at the pendant drop. The surface tension decreased as the nanoparticle concentration increased at the pendant drop surface. This decrease was greater for JPs than for HPs, suggesting enhanced interfacial activity of the Janus nanoparticles as compared to the homogeneous equivalents.

Next, for each particle concentration the shrinking and growing experiment enabled to build a piecewise-like compression isotherm with the pendant drop in air or immersed in decane (see Fig. 14). Given that the adsorption energy of the nanoparticles at the interface is of the order of k_BT when the nanoparticle diameter is in the range of a few nanometers [77], the 3.5 *nm*-diameter HPs and JPs were expected to desorb from the pendant drop interfaces due to thermal fluctuations. However, both HPs and JPs exhibited a significant and stable effect on the surface tension after the THF evaporation and low hysteresis during the growing and shrinking experiments, suggesting that there were nanoparticles at the interface and that they did not desorb from the pendant drop interface over time. Once again, the JPs showed higher interfacial activity than the HPs. Furthermore, the hard disk model (Eq. 13) fitted the HPs compression isotherm and underestimated the JPs results.

$$\Pi(A_p) = \frac{k_B T}{A_p\left(1-\frac{\pi d^2}{4 \cdot A_p}\right)} \tag{13}$$

Eq. 13 is written in terms of the surface pressure Π for a given area per particle at the interface A_p, where k_B is the Boltzmann constant, T is the temperature and d is the hard disk diameter.

Finally, Fernandez-Rodriguez [90] examined the surface activity and the collective behaviour of colloidally stable silver Janus-like particles synthesized following the Sashuk et al. protocol [43] deposited at the water/air interface. The capping ligands were 11-mercaptoundecanoic acid and 1-undecanthiol, hydrophilic and hydrophobic, respectively. They showed an average particle diameter of (100±40) nm and were dispersed in methanol or a mixture of methanol and 2-propanol. The JPs in aqueous media showed colloidal stability at pH values above 5. All experiments of surface activity and collective behavior were performed at pH~6.

Using pendant drop tensiometry, they measured the surface tension of JP monolayers as a function of time, as the spreading solvent was evaporating at different particle surface concentrations and the corresponding adsorption isotherms from the growing and shrinking cycles (surface pressure as a function of area per particle) in a similar way as their previous work [87].

After the evaporation of the spreading solvent, the final surface tension decreased as increasing amounts of JPs were deposited at the interface. As can be seen in Fig. 15, the final surface tension decreased 15 mN/m when the amount of JPs deposited was increased 3.5 times.
They found that the mixture of 2-propanol and methanol as spreading solvent resulted in higher interfacial activity than the methanol alone. This might be due to the formation of complexes between the methanol, 2-propanol and water as reported by Grossmann and Ebert [91].

For each shrinking and growing experiment, the surface pressure Π against the drop area divided by the number of JPs was plotted in Fig. 16. The effective surface tension γ of a JP-laden interface was lower than the surface tension of the bare interface due to the bidimensional osmotic pressure Π generated by the colloidal monolayer.

The hysteresis displayed by the isotherms in Fig. 16 is much smaller than that shown by the isotherms obtained by the conventional Langmuir balance [43]. This indicates that the pendant drop tensiometry enables to measure surface pressure values under experimental conditions very close to the thermodynamic equilibrium and that the migration of JPs deposited at the interface into the aqueous phase was almost negligible. The interface compression produced changes in the surface pressure (around 5 mN/m) at high values of area ($5 \cdot 10^4$ nm^2/particle), which reveals the sensitivity of this technique. Below this point a gas-liquid transition can be identified from the steep rise in the surface pressure. It is noticeable that the complete compression isotherm throughout the range of interfacial area is not single-valued, i.e. the curves obtained with different particle concentration do not overlap perfectly. This can be explained because each part of the compression isotherm corresponds to a different shrinking and growing experiment with different JP amounts in which different self-assembly dynamics could take place. The isotherm collapse is found in Fig. 16 between 10^4 and $2 \cdot 10^4$ nm^2/particle. This collapse corresponds with the close packing of 100 nm particles at the interface, which takes place when the area per particle is $4R^2$ being R the particle radius (a hexagonally close-packed monolayer). Moreover, the surface tension at the collapse state (around 25 mN/m) is in agreement with the reported values for similar JPs [43].
The contact angles of both hemispheres of the JPs are expected to be around 80° and 92°, which does not represent a large wettability contrast in both faces of the JPs used in this study [43]. This reveals that the colloidal stability of the JPs in the bulk solution and at the interface plays a more important role in their interfacial activity rather than the contact angle difference between their faces. Finally, they fitted the Frumkin model [92] (Eq. 14), which relates the surfacepressure (Π) with the area per particle at the interface (A_p).

$$\Pi(A_p) = -\frac{k_B T}{A_0} \ln\left(1 - \frac{A_0}{A_p}\right) - \frac{\beta}{{A_p}^2} \tag{14}$$

where A_0 is the particle geometrical area and β is the interaction constant. The first term was negligible and the second term was fitted with a positive value of $\beta = (1.15\pm0.08)\cdot10^{-26}$ mJ·m^2. The negligible geometrical term in comparison with the high interaction term pointed out to the dominant effect of the lateral attractive interactions between JPs at the water/air interface.

As above mentioned, the shape and wettability of particles have a strong effect on the configuration and interactions between particles placed at fluid-fluid interfaces. In this sense, Park et al [93] performed a very interesting experimental study on the behaviour of double hydrophilic Janus cylinders at air-water and decane-water interfaces. The assemblies of multiple double hydrophilic Janus cylinders at the air-water interface showed structures of nondeterministic assembly behaviours, which are noticeably different from those observed in geometrically anisotropic but chemically homogeneous particles, such as ellipsoids and cylinders [66].

4. Interfacial rheology of Janus particles adsorbed onto liquid interfaces.

The viscosity increase of a solution containing JPs of SiO_2 and Fe_3O_4 when it is applied an external AC electric and magnetic fields due to the formation of chains was studied by Ren and Kretzschmar [94]. However these measurements referred to particles in the bulk of a solution. In order to study the viscosity and elasticity of the JPs at a fluid-fluid interface it is necessary to study the interfacial rheology of the interface [95]. The dilatational rheology of the colloidal layers formed at the pendant drop interface can be measured with the oscillating pendant drop tensiometry. An oscillatory perturbation is applied to the interface by injecting and extracting volume to the drop. The system records the response of the surface tension to the area deformation. The average dilatational modulus (E), the mean surface tension (γ) andthe surface dilatational viscosity (η_d) are obtained from this response [95]. To obtain the dilatational modulus it is required a quasi-equilibrium drop shape for the calculation of the surface tension to avoid excessive perturbation of the colloidal monolayer and the departure from the viscoelastic linear region as discussed by Hilles et al. [96]. However, above this viscoelastic linear region it is still possible to obtain an average dilatational modulus in which the main contribution comes from the dilatational modulus in the viscoelastic linear region. Fernandez et al. [90] studied the interfacial rheology of silver Janus-like particles in water/air interface. The initial pendant drop volume was 20 μL or 10 μL, which depended on the surface particle concentration. In all rheology experiments, they applied a sinusoidal oscillation in the pendant drop volume with 1 μL amplitude and a frequency of 0.1 Hz, which was above the viscoelastic linear region. They distinguished two different behaviours depending on the spreading agents used in the deposition of the JPs. The average dilatational modulus changed dramatically when the colloidal monolayer collapsed (from E = (62±2) mN/m to (620±50) mN/m) when 2-propanol and methanol mixture was used as spreading agent. On the other hand, when methanol only was used as spreading agent, the

average dilatational modulus was low in comparison and did not change significantly after the collapse (always below E < 28 mN/m). In all cases the average dilatational viscosity was very low (η_d< 14 mN/ms). The values of E and η_d obtained upon these states agree, which indicates that the collective behaviour of the JPs is practically independent of the geometrical arrangement of particles in the colloidal monolayer. This illustrates again the decisive role played by the spreading agent. The collapsed monolayer was reproduced to lower values of surface pressure using methanol (around 25 mN/m) instead of methanol (around 45 mN/m). The elastic network formed by the JPs at the interface at high surface pressure is strongly influenced by the presence of solvent molecular clusters established with water [91].

5. Conclusion.

Since de Gennes published in 1992 his inspiring work coining the term Janus particle (JP), there has been a strong effort to develop different routes to synthesize JPs. These particles with two spatial domains of different wettability are able to stabilize Pickering emulsions rather than homogeneous particles (HPs) due to the desorption energy of JPs, three times greater than for HPs. Different methods are being used to characterize the interfacial activity of JPs-laden interfaces as the Langmuir balance, but often the synthesis produces small amount of JPs, not enough to perform an experiment of Langmuir balance. Otherwise, pendant drop tensiometry allows exploring the interfacial activity of JPs in different fluid-fluid interfaces with much less number of JPs. Furthermore, if the particles are deposited onto the interface dispersed in a spreading solvent, the necessary quantity of JPs is even lower and the evaporation of the spreading solvent provides enough energy to place the JPs at the interface faster than the diffusion-driven adsorption of JPs from the bulk of the pendant drop. Also, the pendant drop tensiometry enables to easily perform dilatational surface rheology to characterize the collective behaviour of the JPs at the interface of the pendant drop. In all the theoretical and experimental works there are several parameters that conditions the interfacial activity of the JPs: shape, morphology and distribution of the spatial domains which confers the Janus character to the particle, spreading solvent, colloidal stability, charge and composition of the JP. Finally, regardless of the synthesis and characterization methods, the JPs show an enhanced interfacial activity compared to the corresponding HPs.

Acknowledgement

This work was supported by the Spanish MINECO (projects MAT2011-23339 and MAT2013-44429-R), by “Junta de Andalucía” and FEDER (projects P10-FQM-5977 and P12-FQM-1443).

References

1. de Gennes PG. Soft Matter. Science 1992; 256:495-7.

2. Yan J, Bae SC, Granick S. Rotating crystals of magnetic Janus colloids. Soft Matter 2015; 11:147-53.
3. Bradley M, Rowe J. Cluster formation of Janus polymer microgels. Soft Matter 2009; 5:3114-9.
4. Onishi S, Tokuda M, Suzuki T, Minami H. Preparation of Janus particles with different stabilizers and formation of one-dimensional particle arrays. Langmuir 2015; 31:674-8.
5. Kaewsaneha Ch, Tangboriboonrat P, Polpanich D, Eissa D, Elaissari A. Janus Colloidal Particles:Preparation, Properties, and Biomedical Applications. ACS Appl. Mater. Interfaces 2013; 5:1857-69.
6. Gao Y, Yu Y. Macrophage Uptake of Janus Particles Depends upon Janus Balance. Langmuir 2015; 31(9):2833-8.
7. Tu F, Lee D. Shape-changing and amphiphilicity-reversing Janus particles with pH-responsive surfactant properties. J. Am. Chem. Soc. 2014; 136(28):9999-10006.
8. Cui F, Lin J, Li Y, Li Y, Wu H, Yu F, Jia M, Yang X, Wu S, Xie L, Ye S, Luo F, Hou Z. Mol. Pharmaceutics 2015; 12(4):1318-27.
9. Garbuzenko OB, Winkler J, Tomassone MS, Minko T. Biodegradable Janus nanoparticles for local pulmonary delivery of hydrophilic and hydrophobic molecules to the lungs. Langmuir 2014; 30(43):12941-9.
10. Mammen L, Bley K, Papadopoulos P, Schellenberger F, Encinas N, Butt HJ, Weiss CK, Vollmer D. Functional superhydrophobic surfaces made of Janus micropillars. Soft Matter 2015; 11(3):506-15.
11. Nedev S, Carretero-Palacios S, Kuhler P, Lohmuller Th, Urban AS, Anderson LJE, Feldman J. An optically controlled microscale elevator using plasmonic Janus particles. ACS Photonics 2015; 2(4):491-6.
12. Bormashenko E, Bormashenko Y, Pogreb R, Gendelman O. Janus Droplets:Liquid Marbles Coated with Dielectric/Semiconductor Particles. Langmuir 2011; 27:7-10.
13. Teo BM, Suh SK, Hatton TA, Ashokkumar M, Grieser F. Sonochemical Synthesis of Magnetic Janus Nanoparticles. Langmuir 2011; 27:30-3.
14. Yuet KP, Hwang DK, Haghgooie R, Doyle PS. Multifunctional Superparamagnetic Janus Particles. Langmuir 2010; 26:4281-7.
15. Ren B, Ruditskiy A, Song JH, Kretzschmar I. Assembly behavior of iron oxide-capped Janus particles in a magnetic field. Langmuir 2012; 28(2):1149-56.
16. Bharti B, Velev OD. Assembly of Reconfigurable Colloidal Structures by Multidirectional Field-Induced Interactions. Langmuir 2015; Article ASAP,DOI:10.1021/la504793y.
17. Smoukov SK, Gangwal S, Marquez M, Velev OD. Reconfigurable responsive structures assembled from magnetic Janus particles. Soft Matter 2009; 5:1285-92.
18. Gangwal S, Cayre OJ, Velev OD. Dielectrophoretic Assembly of Metallodielectric Janus Particles in AC Electric Fields. Langmuir 2008; 24(23):13312-20.
19. Komazaki Y, Hirama H, Torii T. Electrically and magnetically dual-driven Janus particles for handwriting-enabled electronic paper. J. Appl. Phys. 2015; 117:154506.
20. Hu J, Zhou S, Sun Y, Fang X, Wu L. Fabrication, properties and application of Janus particles. Chem. Soc. Rev. 2012; 41:4356-78.
21. Perro A, Reculusa S, Ravaine S, Bourgeat-Lami E, Duguet E. Design and synthesis of Janus micro- and nanoparticles. J. Mater. Chem. 2005; 15:3745-60.
22. Suzuki D, Tsuji S, Kawaguchi H. Janus microgels prepared by surfactant-free Pickering emulsion-based modification and their assembly. J. Am. Chem. Soc. 2007; 129:8088-9.
23. Binks BP. Particles as surfactants-similarities and differences. Curr. Opin. Colloid Interface Sci. 2002; 7:21-41.
24. Lattuada M, Hatton TA. Synthesis, Properties and Applications of Janus Nanoparticles. Nano Today 2011; 6(3):286-308.

25. Casagrande C, Fabre P, Raphaël E, Veyssié M. “Janus beads”:Realization and behaviour at water/oil interfaces. Europhys. Lett. 1989; 9(3):251-5.
26. Kumar A, Park BJ, Tu F, Lee D. Amphiphilic Janus particles at fluid interfaces. Soft Matter 2013; 9:6604-17.
27. Pradhan S, Xu L, Chen S. Janus nanoparticles by interfacial engineering. Adv. Funct. Mater. 2007; 17:2385-92.
28. Glaser N, Adams DJ, Böker A, Krausch G. Janus particles at liquid-liquid interfaces. Langmuir 2006; 22(12):5227-9.
29. Walther A, Müller AHE. Janus Particles:Synthesis, Self-Assembly, Physical Properties, and Applications. Chem. Rev. 2013; 113:5194-261.
30. Chen B, Jia Y, Gao Y, Sanchez L, Anthony SM, Yu Y. Janus particles as artificial antigen-presenting cells for T cell activation. ACS Appl. Matter. Interfaces 2014; 6(21):18435-9.
31. Binks BP, Fletcher PDI. Particles Adsorbed at the Oil-Water Interface:A Theoretical Comparison between Spheres of Uniform Wettability and Janus Particles. Langmuir 2001; 17:4708-10.
32. Hirose Y, Komura S, Nonomura Y. Adsorption of Janus particles to curved interfaces. J. Chem. Phys. 2007; 127:054707.
33. Jiang S, Granick S. Janus balance of amphiphilic colloidal particles. J. Chem. Phys. 2007; 127:161102-4.
34. Ruhland TM, Gröschel AH, Walther A, Müller AHE. Janus Cylinders at Liquid-Liquid Interfaces. Langmuir 2011; 27(16):9807-14.
35. Ruhland TM, Grüschel AH, Ballard N, Skelhon TS, Walther A, Müller AHE, Bon SAF. Influence of Janus Particle Shape on Their Interfacial Behavior at Liquid-Liquid Interfaces. Langmuir 2013; 29:1388-94.
36. Larson-Smith K, Pozzo DC. Pickering Emulsions Stabilized by Nanoparticle Surfactants. Langmuir 2012; 28:11725-32.
37. Reguera J, Ponomarev E, Geue T, Stellacci F, Bresme F, Moglianetti M. Contact angle and adsorption energies of nanoparticles at the air-liquid interface determined by neutron reflectivity and molecular dynamics. Nanoscale 2015; 7:5665-73.
38. Xu H, Liu X, Su G, Zhang B, Wang D. Electrostatic Repulsion-Controlled Formation of Polydopamine-Gold Janus Particles. Langmuir 2012; 28:13060-5.
39. Fujii S, Yokoyama Y, Miyanari Y, Shiono T, Ito M, Yusa S, Nakamura Y. Micrometer-Sized Gold Silica Janus Particles as Particulate Emulsifiers. Langmuir 2013; 29:5457-65.
40. Meng X, Guan Y, Zhang Z, Qiu D. Fabrication of a Composite Colloidal Particle with Unusual Janus Structure as a High-Performance Solid Emulsifier. Langmuir 2012; 28:12472-8.
41. Zhang J, Jin J, Zhao H. Surface-Initiated Free Radical Polymerization at the Liquid-Liquid Interface:A One-Step Approach for the Synthesis of Amphiphilic Janus Silica Particles. Langmuir 2009; 25:6431-7.
42. Liu L, Ren M, Yang W. Preparation of Polymeric Janus Particles by Directional UV-Induced Reactions. Langmuir 2009; 25:11048-53.
43. Sashuk V, Hołyst R, Wojciechowski T, Fiałkowski M. Close-packed monolayers of charged Janus-type nanoparticles at the air-water interface. J. Colloid Interface Sci. 2012; 375(1):180-6.
44. Garbin V, Crocker JC, Stebe KJ. Particles at interfaces. J. Colloid Interface Sci. 2012; 387:1-11.
45. Park BJ, Brugarolas T, Lee D. Janus particles at an oil-water interface. Soft Matter 2011; 7:6413-7.
46. Nie L, Liu S, Shen W, Chen D, Jiang M. One-pot synthesis of amphiphilic polymeric janus particles and their self-assembly into supermicelles with a narrow size distribution. Angew. Chem. Int. Ed. Engl. 2007; 46(33):6321-4.
47. Chen Q, Whitmer JK, Jiang S, Bae1 SC, Luijten E, Granick S. Supracolloidal Reaction Kinetics of Janus Spheres. Science 2011; 331(6014):199-202.

48. Yu C, Zhang J, Granick S. Selective Janus Particle Assembly at Tipping Points of Thermally-Switched Wetting. Angew. Chem. Int. Ed. Engl 2014; 53(17):4364-7.
49. Shah AA, Schultz B, Zhang W, Glotzer SC, Solomon MJ. Actuation of shape-memory colloidal fibres of Janus ellipsoids. Nat. Mater. 2015; 14:117-24.
50. Beltran-Villegas DJ, Schultz BA, Nguyen NH, Glotzer SC, Larson RG. Phase behavior of Janus colloids determined by sedimentation equilibrium. Soft Matter 2014; 10(26):4593-602.
51. Luo M, Olivier GK, Frechette J. Electrostatic interactions to modulate the reflective assembly of nanoparticles at the oil-water interface. Soft Matter 2012; 8(47):11923-32.
52. Hong L, Cacciuto A, Luijten E, Granick S. Clusters of charged Janus spheres. Nano Lett. 2006; 6(11):2510-4.
53. Santos A, López de Haro M, Yuste S. An Accurate and Simple Equation of State for Hard Disks. J. Chem. Phys. 1995; 103:4622-5.
54. Isa L, Amstad E, Schwenke K, Del Gado E, Ilg P, Kroger M, Reimhult E. Adsorption of Core-Shell Nanoparticles at Liquid-Liquid Interfaces. Soft Matter 2011; 7:7663-75.
55. Liu Z, Guo R, Xu G, Huang Z, Yan LT. Entropy-Mediated Mechanical Response of the Interfacial Nanoparticle Patterning. Nano Lett. 2014; 14(12):6910-6.
56. Lee KJ, Yoon J, Lahann J. Recent advances with anisotropic particles. Curr. Opin. Colloid Interface Sci. 2011; 16:195.
57. Cheung DL, Bon SAF. Stability of Janus nanoparticles at fluid interfaces. Soft Matter 2009; 5:3969-76.
58. Aveyard R. Can Janus particles give thermodynamically stable Pickering emulsions? Soft Matter 2012; 8:5233-40.
59. Tu F, Park BJ, Lee D. Thermodynamically Stable Emulsions Using Janus Dumbbells as Colloid Surfactants. Langmuir 2013: 29(41):12679-87.
60. Park BJ, Lee D. Equilibrium orientation of nonspherical Janus particles at fluid-fluid interfaces. ACS Nano 2012; 6(1):782-90.
61. Luu XC, Yu J, Striolo A. Ellipsoidal Janus Nanoparticles Adsorbed at the Water-Oil Interface: Some Evidence of Emergent Behavior. J. Phys. Chem. B 2013; 117(44):13922-9.
62. Rezvantalab H, Shojaei-Zadeh SH. Role of geometry and amphiphilicity on capillary-induced interactions between anisotropic Janus particles. Langmuir 2013; 29(48):14962-70.
63. Luu XC, Striolo A. Ellipsoidal Janus nanoparticles assembled at spherical oil/water interfaces. J. Phys. Chem. B 2014; 118(47):13737-43.
64. Güell O, Sagués F, Tierno P. Magnetically driven Janus micro-ellipsoids realized via asymmetric gathering of magnetic charge. Adv. Mater 2011; 23(32):3674-9.
65. Basavaraj MG, Fuller GG, Fransaer J, Vermant J. Packing, flipping and buckling transitions in compressed monolayers of ellipsoidal latex particles. Langmuir 2006; 22(15):6605-12.
66. Basavaraj MG, Fransaer J, Vermant J. Self-assembly and rheology of ellipsoidal particles at interfaces. Langmuir 2009; 25(5):2718-28.
67. Basavaraj MG, Vandebril S, Fransaer J, Vermant J. Exploiting particle shape in solid stabilized emulsions. Soft Matter 2009; 5:1717-27.
68. Gao HM, Lu ZY, Liu H, Sun ZY, An LJ. Orientation and surface activity of Janus particles at fluid-fluid interfaces. J. Chem. Phys. 2014; 141(13):134907.
69. Detrich Á, Deák A, Hild E, Kovács AL, Hórvölgyi Z. Langmuir and Langmuir-Blodgett Films of Bidisperse Silica Nanoparticles. Langmuir 2010; 26:2694-9.
70. Kim JY, Raja S, Stellacci F. Evolution of Langmuir Film of Nanoparticles Through Successive Compression Cycles. Small 2011; 7:2526-32.
71. Pradhan S, Brown L, Konopelski J, Chen S. Janus Nanoparticles:Reaction Dynamics and NOESY Characterization. J. Nanopart. Res. 2009; 11:1895-903.

72. Centrone A, Hu Y, Jackson AM, Zerbi G, Stellacci F. Phase separation on mixed-monolayer-protected metal nanoparticles:a study by infrared spectroscopy and scanning tunneling microscopy. Small 2007; 3(5):814-7.
73. Jackson AM, Myerson JW, Stellacci F. Spontaneous assembly of subnanometer-ordered domains in the ligand shell of monolayer-protected nanoparticles. Nat Mater. 2004; 3(5):330-6.
74. Rotenberg Y, Boruvka L, Neumann AW. Determination of surface tension and contact angle from the shapes of axisymmetric fluid interfaces. J. Colloid Interface Sci. 1983; 93:169-83.
75. Cabrerizo-Vílchez MA, Wege HA, Holgado-Terriza JA, Neumann AW. Axisymmetric drop shape analysis as penetration Langmuir balance. Rev. Sci. Instrum. 1999; 70(5):2438-44.
76. Kwok DY, Vollhardt D, Miller R, Li D, Neumann AW. Axisymmetric drop shape as a film balance. Colloids Surf. A 1994; 88(1):51-58.
77. Ferdous S, Ioannidis M, Henneke D. Adsorption Kinetics of Alkanethiol-Capped Gold Nanoparticles at the Hexane-Water Interface. J. Nanopart. Res. 2011; 13:6579-89.
78. Yu H, Chen M, Rice PM, Wang SX, White RL, Sun SH. Dumbbell-Like Au-Fe3O4 Nanoparticles for Target-Specific Platin Delivery. Nano Lett. 2005; 5:379-82.
79. Pieranski P. Two-Dimensional Interfacial Colloidal Crystals. Phys. Rev. Lett. 1980; 45:569-72.
80. Morgan AR, Ballard N, Rochford LA, Nurumbetov G, Skelhon TS, Bon SAF. Understanding the Multiple Orientations of Isolated Superellipsoidal Hematite Particles at the Oil-Water Interface. Soft Matter 2013; 9:487-91.
81. Maestro A, Bonales, LJ, Ritacco H, Rubio RG, Ortega F. Effect of the spreading solvent on the three-phase contact angle of microparticles attached at fluid interfaces. Phys. Chem. Chem. Phys. 2010, 12, 14115-14120.
82. Stamou D, Duschl C, Johannsmann D. Long-range attraction between colloidal spheres at the air-water interface:The consequence of an irregular meniscus. Phys. Rev. E:Stat. Phys., Plasmas, Fluids, Relat. Interdiscip. Top. 2000; 62:5263-72.
83. Martínez-López F, Cabrerizo-Vílchez MA, Hidalgo-Álvarez R. Colloidal Interaction at the Air-Liquid Interface. J Colloid Interface Sci. 2000; 232(2):303-10.
84. Frost DS, Nofen EM, Dai LL. Particle self-assembly at ionic liquid-based interfaces. Adv. Colloid Interface Sci. 2014; 206:92-105.
85. Poulichet V, Garbin V. Ultrafast desorption of colloidal particles from fluid interfaces. Proc. Natl. Acad. Sci. USA. 2015;112(19):5932-7.
86. Tran N, Mulet X, Hawley AM, Conn CE, Zhai J, Waddington LJ, Drummond CJ. First Direct Observation of Stable Internally Ordered Janus Nanoparticles Created by Lipid Self-Assembly. Nano Lett. 2015; Article ASAP,DOI:10.1021/acs.nanolett.5b01751.
87. Fernandez-Rodriguez MA, Song Y, Rodriguez-Valverde MA, Chen S, Cabrerizo-Vilchez MA, Hidalgo-Alvarez R. Comparison of the Interfacial Activity between Homogeneous and Janus Gold Nanoparticles by Pendant Drop Tensiometry. Langmuir 2014; 30:1799-804.
88. Brust M, Walker M, Bethell D, Schiffrin DJ, Whyman R. Synthesis of Thiol-Derivatised Gold Nanoparticles in a Two-Phase Liquid-Liquid System. J. Chem. Soc., Chem. Commun. 1994; 0:801-2.
89. Xu LP, Pradhan S, Chen S. Adhesion Force Studies of Janus Nanoparticles. Langmuir 2007; 23:8544-8.
90. Fernandez-Rodriguez MA, Rodriguez-Valverde MA, Cabrerizo-Vilchez M, Hidalgo-Alvarez R. Surface activity and collective behaviour of colloidally stable Janus-like particles at the air-water interface. Soft Matter 2014; 10(19):3471-6.
91. Grossmann GH, Ebert KH. Formation of clusters in 1-propanol-water-mixtures. Ber. Bunsenges. Phys. Chem. 1981; 85:1026-37.
92. Rusanov AI. New theory of equation of state for surface monolayer. J. Chem. Phys. 2004; 120(22):10736-48.
93. Park BJ, Choi ChH, Kang SM, Tettey KE, Lee ChS, Lee D. Double hydrophilic Janus cylinders at an

air-water interface. Langmuir 2013; 29(6):1841-9.
94. Ren B, Kretzschmar I. Viscosity-Dependent Janus Particle Chain Dynamics. Langmuir 2013; 29(48):14779-86.
95. Maldonado Valderrama J, Wege H, Rodríguez Valverde MA, Gálvez Ruiz MJ, Cabrerizo Vílchez MA. Comparative study of adsorbed and spread beta-Casein monolayers at the water-Air interface with the pendant drop technique. Langmuir 2003; 19:8436-42.
96. Hilles H, Monroy F, Bonales LJ, Ortega F, Rubio RG. Fourier-transform rheology of polymer Langmuir monolayers: Analysis of the non-linear and plastic behaviors. Adv. Colloid Interface Sci. 2006; 122:67-77.

Fig. 1. Geometry of a Janus particle within an oil-water interface. The relative areas of the polar and apolar particle surface regions are parametrized by the angle α. The immersion depth of the particle in the oil-water interface is parametrized by the angle β. Reprinted with permission from [31]. Copyright (2001) American Chemical Society.

Fig. 2. Variation of particle desorption energy with area-weighted average contact angle forparticles of radius 10 nm and α = 90°. The oil-water tension was set to 36 $mN \cdot m^{-1}$. In order of increasing desorption energies, the curves refer to Δθ = 0° (the homogeneous particle case), 20, 40, 60 and 90°. Reprinted with permission from [31]. Copyright (2001) American Chemical Society.

Fig. 3. The dimensionless adsorption energy g_i as a function of the contact angle θ for ε = 0 (solid line), ε = 0.2 (dashed line), and ε = 0.4 (dotted line). The other parameters are α = π/2, $\gamma_A = \frac{\gamma_{1A}-\gamma_{2A}}{\gamma_{12}}$= -0.25, and $\gamma_B = \frac{\gamma_{1B}-\gamma_{2B}}{\gamma_{12}}$ = 0.25. The minimum denoted by the filled circle coincides with the anchoring angle (indicated by an arrow) when ε = 0 and 0.2, while it is given by Young's equation for ε = 0.4. Reprinted with permission from [32]. Copyright [2007], AIP Publishing LLC.

Fig. 4. Free energy U_F as a function of the particle distance from the interface at different θ_{int} with the parameter β = 0.08 for Janus spheres, Janus rods, and Janus disks. The schematics of Janus particles show their final orientations at the fluid-fluid interface. The error bars represent one standard deviation from the average. The aspect ratio of Janus particles is 1, 3.3, and 0.3 for Janus sphere, rod, and disk, respectively. Reprinted with permission from [68]. Copyright [2014], AIP Publishing LLC.

Fig. 5. Time evolution of interfacial tension γ for Janus particles with different shapes and different β. In these simulations, the aspect ratio of Janus particles is 1, 3.3, and 0.3 for Janus sphere, rod, and disk, respectively. Reprinted with permission from [68]. Copyright [2014], AIP Publishing LLC.

Fig. 6. The Π–A isotherm of a monolayer of 10Au (+) NPs. The monolayer is compressed at ~100 nm^2/NP. This point (marked in red) corresponds to the close-packed hexagonal structure. (b) Photograph of a glass slide covered with 10Au (+) NPs using the up-stroke deposition method. Reprinted from [43], Copyright (2012), with permission from Elsevier.

Fig. 7. Interfacial tension in terms of time. Water was used as the drop phase, and n-hexane was used as the ambient phase in which the nanoparticles were diluted. (NP: homogeneous nanoparticles; JP: Janus particles. The gold moieties were modified using dodecanethiol (DDT) or octadecanethiol (ODT).). Reprinted with permission from [28]. Copyright (2006) American Chemical Society.

Fig. 8. Schematic representation of Janus particles at the hexane-water interface (red: gold part; gray: iron oxide part). Reprinted with permission from [28]. Copyright (2006) American Chemical Society.

Fig. 9. Influence of the length of Janus cylinders on the interfacial tension. (A) Interfacial tension isotherms of solutions of Janus cylinders in dioxane at the PFO/dioxane interface and (B) in DMSO at the PFO/DMSO interface (c = 1 g/L). Interfacial tension isotherms for uncrosslinked SBM and homogeneous BS core-shell cylinders are included. (C) Relative decrease of quasi-equilibrium interfacial tensions as a function of the cylinder length for both solvent systems. Reprinted with permission from [34].Copyright (2011) American Chemical Society.

Fig. 10. Left top: adsorption curves in linear and logarithmic presentation. (A-H) Series of TEM images (obtained from lacey grids) of 2300 nm Janus cylinders (1 g/L) adsorbing at the PFO/dioxane interface at different times as noted in the interfacial isotherms (scale bars: 1 μm). Reprinted with permission from [34]. Copyright (2011) American Chemical Society.

Fig. 11. Overview of Possible Janus Particle Architectures: (A) Spheres, (B) Cylinders, and (C) Discs. Reprinted with permission from [35]. Copyright (2013) American Chemical Society.

Fig. 12. Influence of the Janus particle shape on the interfacial tension. (A) Interfacial tension isotherms of solutions of Janus particles in toluene at a water/toluene interface. (B) Logarithmic representation of the data in (A). Reprinted with permission from [35]. Copyright (2013) American Chemical Society.

Fig. 13. Surface tension evolution over time after depositions of gold HPs and JPs at the surface of an initial 5 μl MilliQ water pendant drop and subsequent growing at a 0.08 $\mu l/s$ rate up to 20 μl. Each line corresponds to different depositions with different number of HPs or JPs. After the solvent evaporation, the surface tension remained stable. Reprinted with permission from [87]. Copyright (2014) American Chemical Society.

Fig. 14. Surface pressure against the area per particle for different number of gold JPs (red dots) and HPs (black dots) deposited at the interface. Each black or red symbol corresponds to a single JP or HP deposition at the interface of the pendant drop. The solid line is the hard disks model (Eq. 13) for disks of 1nm diameter. Reprinted with permission from [87]. Copyright (2014) American Chemical Society.

Fig. 15. Surface tension γ as a function of time for different silver Janus-like particle concentrations during the formation of the pendant drop and the subsequent deposition of the monolayer [90]. Reproduced by permission of The Royal Society of Chemistry.

Fig. 16. Surface pressure as a function of surface area per particle for different silver Janus-like particle concentrations using methanol as spreading agent. The gray line is an eye guide and the dashed line the fitting with the Frumkin model [90]. Reproduced by permission of The Royal Society of Chemistry.

Fig. 1:

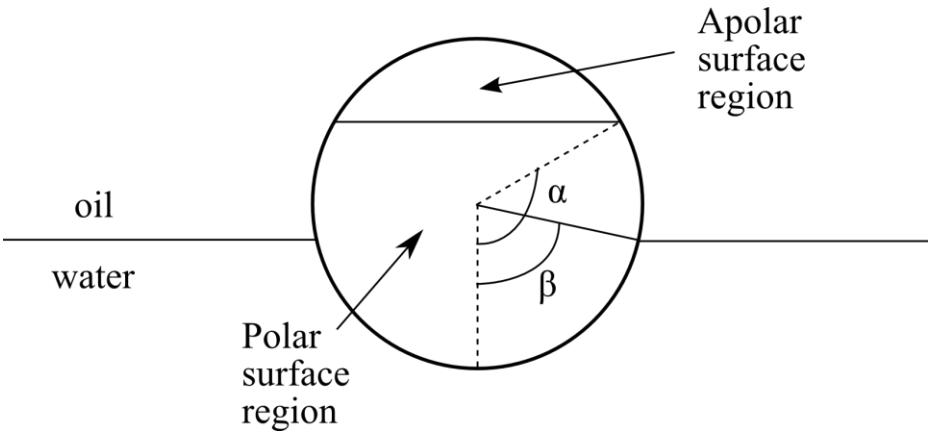
Apolar
surface
region
oil
water
α
β
Polar
surface
region

Fig. 2:

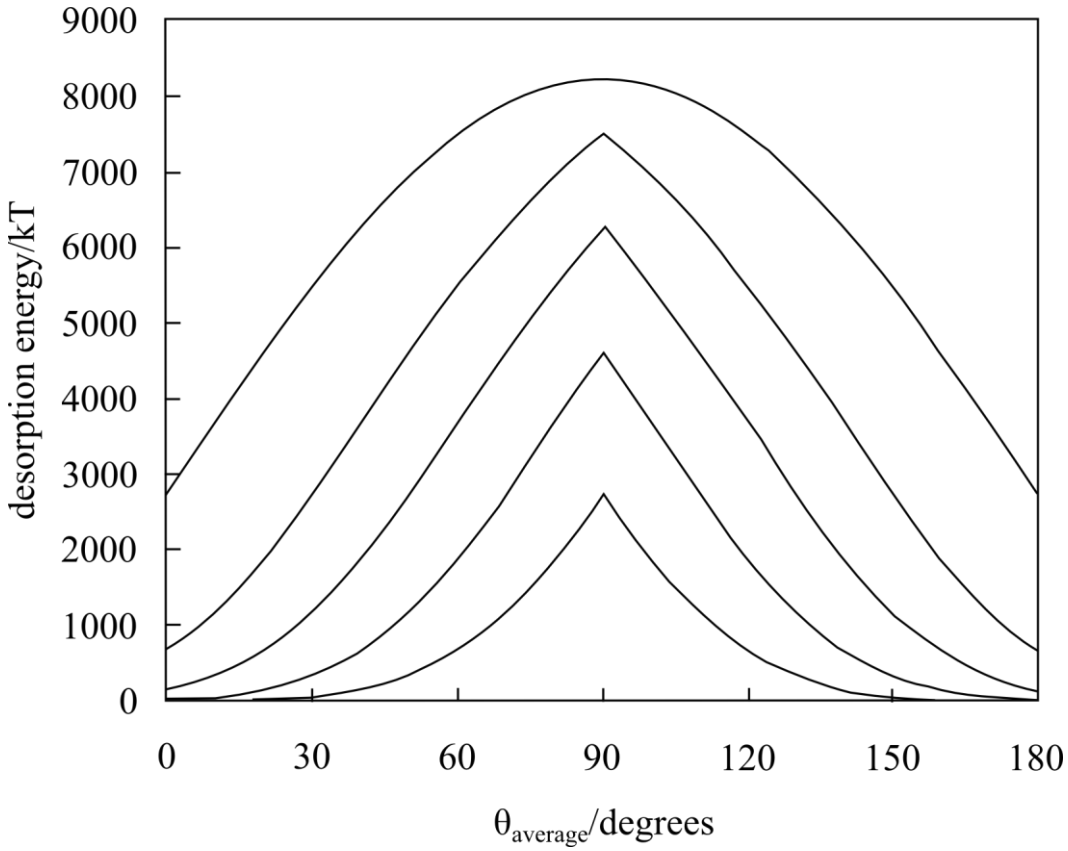
9000
8000
7000
6000
5000
4000
3000
2000
1000
0
desorption energy/kT
0
30
60
90
120
150
180
θaverage/degrees

Fig. 3:

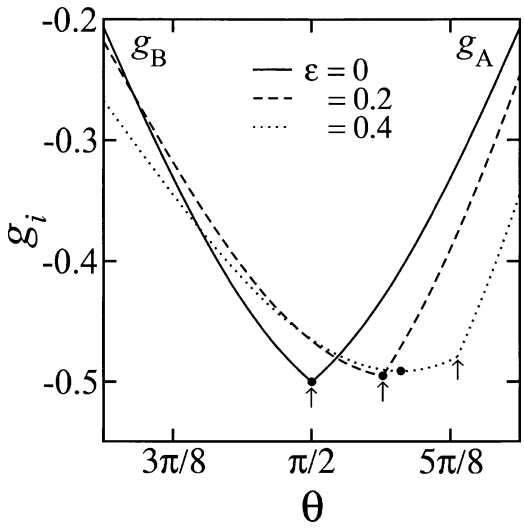
-0.2
-0.3
-0.4
-0.5
g_i
g_B
g_A
ε = 0
= 0.2
= 0.4
3π/8
π/2
5π/8
θ

Fig. 4:

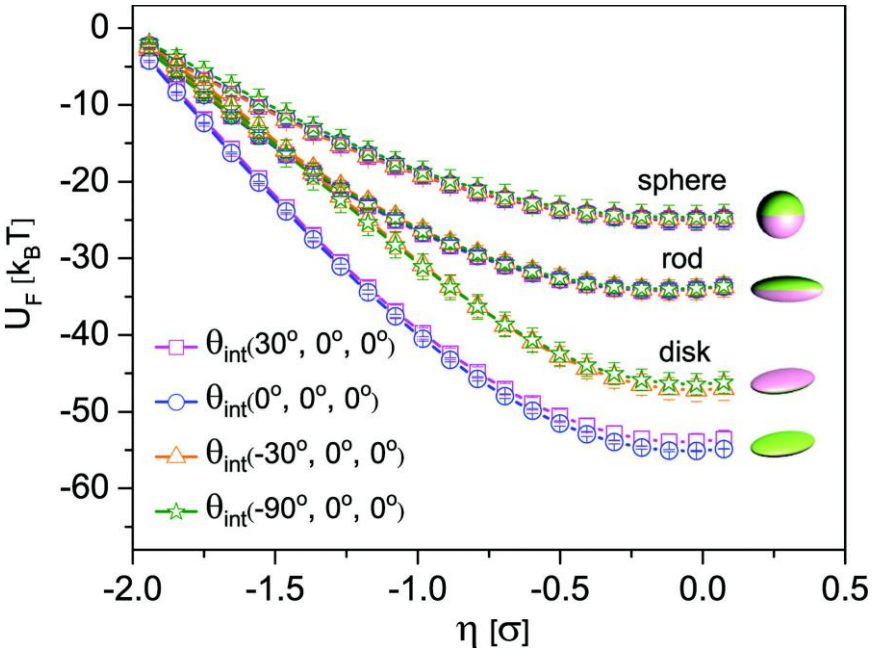
0
-10
-20
-30
-40
-50
-60
U_F [k_BT]
sphere
rod
disk
θ_{int}(30°, 0°, 0°)
θ_{int}(0°, 0°, 0°)
θ_{int}(-30°, 0°, 0°)
θ_{int}(-90°, 0°, 0°)
-2.0
-1.5
-1.0
-0.5
0.0
0.5
η [σ]

Fig. 5:

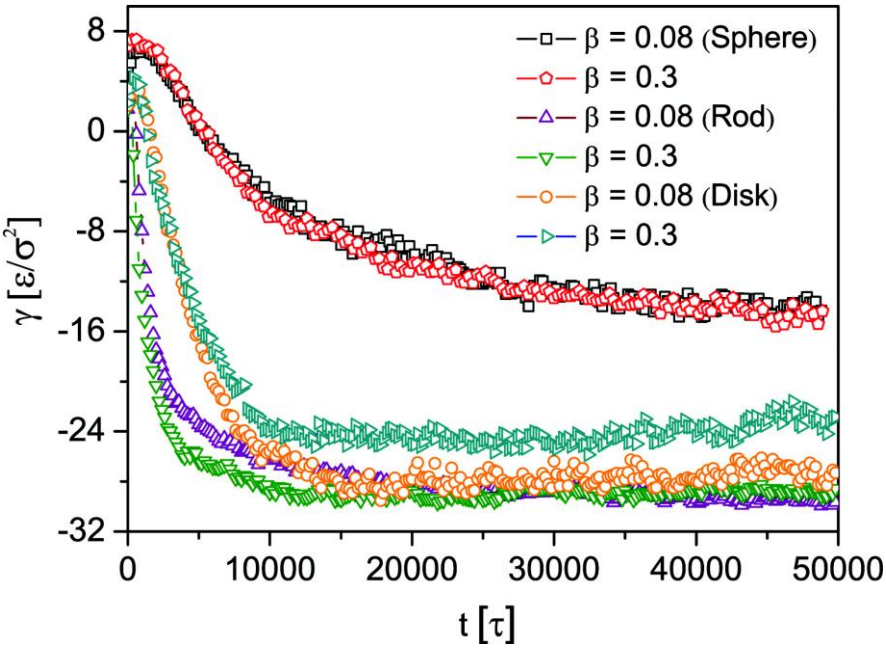
β = 0.08 (Sphere)
β = 0.3
β = 0.08 (Rod)
β = 0.3
β = 0.08 (Disk)
β = 0.3
γ [ε/σ²]
t [τ]
8
0
-8
-16
-24
-32
0
10000
20000
30000
40000
50000

Fig. 6:

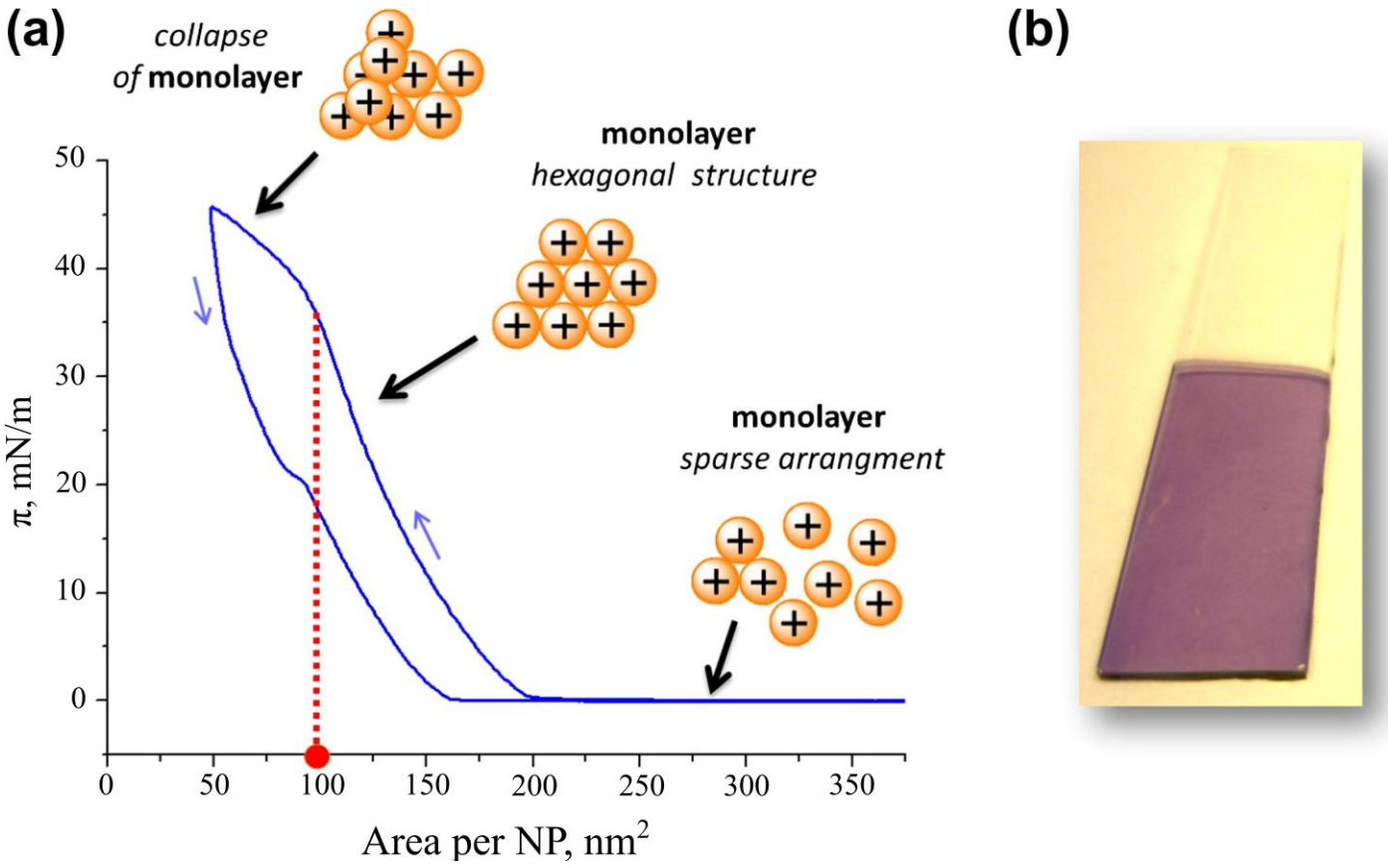
(a)
collapse
of monolayer
monolayer
hexagonal structure
monolayer
sparse arrangment
π, mN/m
Area per NP, nm²
(b)

Fig. 7:

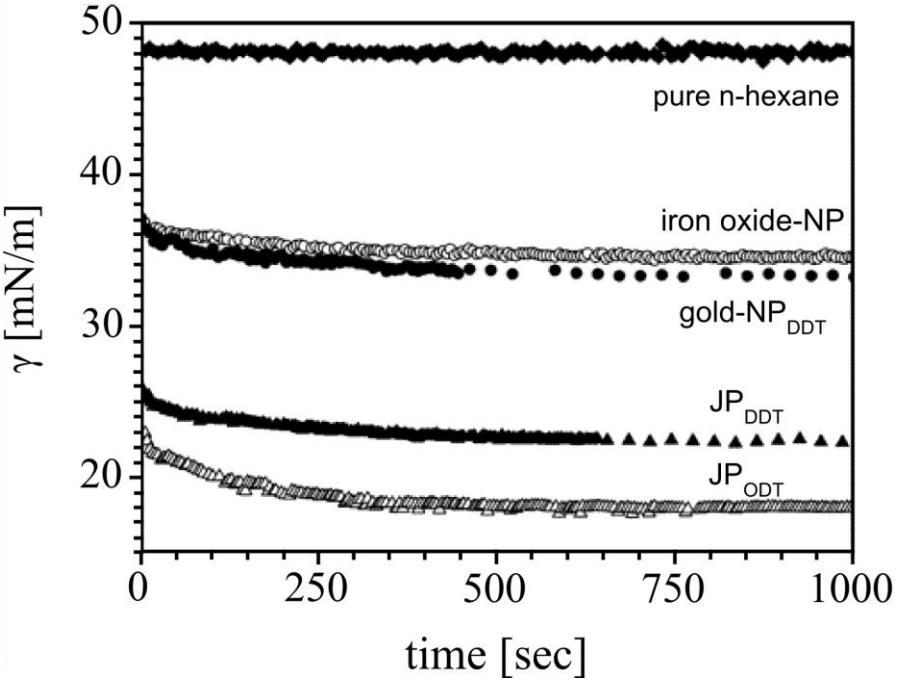
50
40
30
20
γ [mN/m]
0
250
500
750
1000
time [sec]
pure n-hexane
iron oxide-NP
gold-NP$_{DDT}$
JP$_{DDT}$
JP$_{ODT}$

Fig. 8:

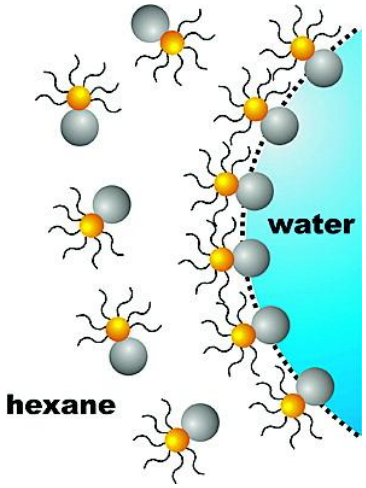
water
hexane

Fig. 9:

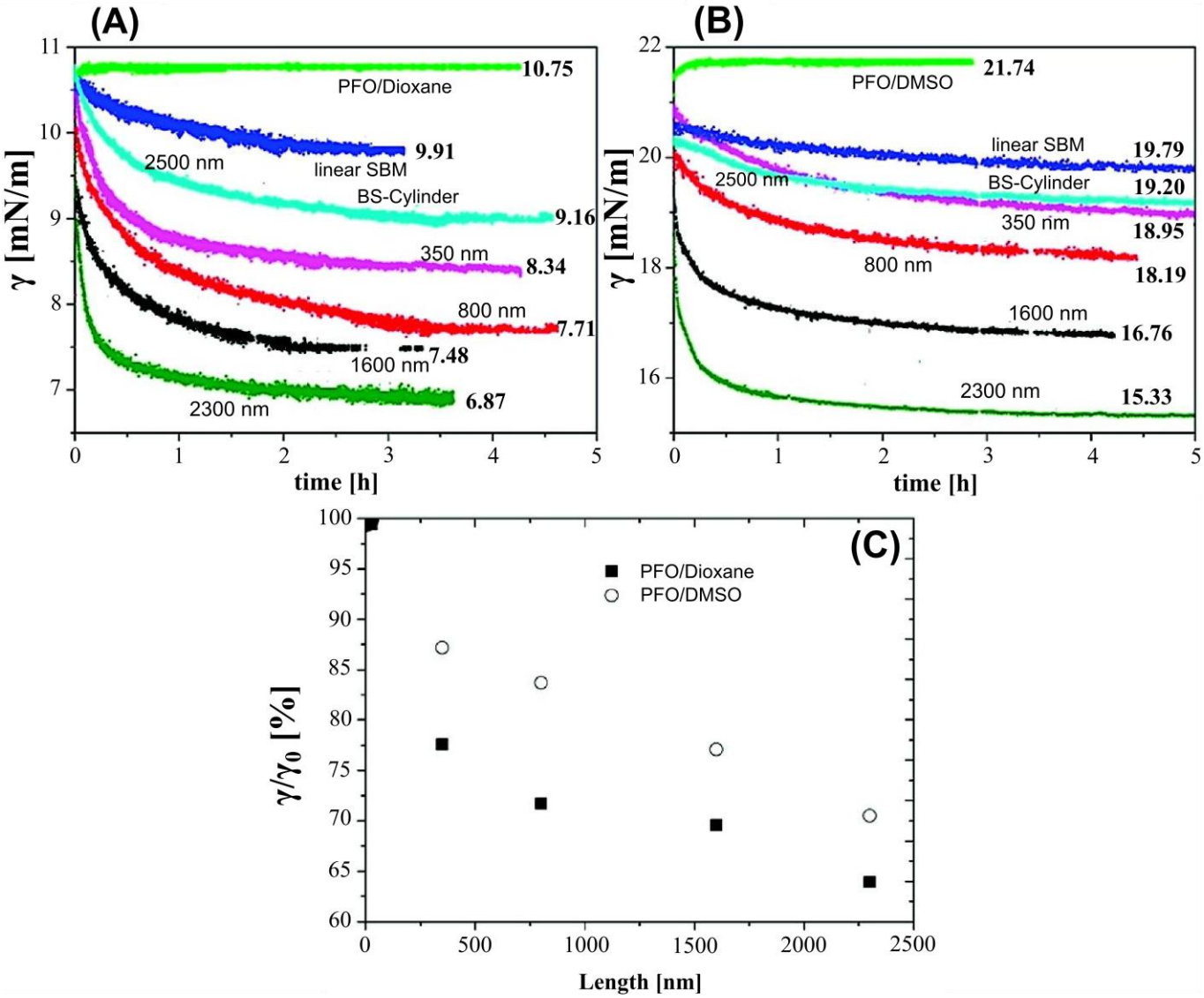
(A)
γ [mN/m]
time [h]
PFO/Dioxane
10.75
2500 nm
linear SBM
9.91
BS-Cylinder
9.16
350 nm
8.34
800 nm
7.71
1600 nm
7.48
2300 nm
6.87
(B)
γ [mN/m]
time [h]
PFO/DMSO
21.74
linear SBM
19.79
2500 nm
BS-Cylinder
19.20
350 nm
18.95
800 nm
18.19
1600 nm
16.76
2300 nm
15.33
(C)
γ/γ0 [%]
Length [nm]
PFO/Dioxane
PFO/DMSO

Fig. 10:

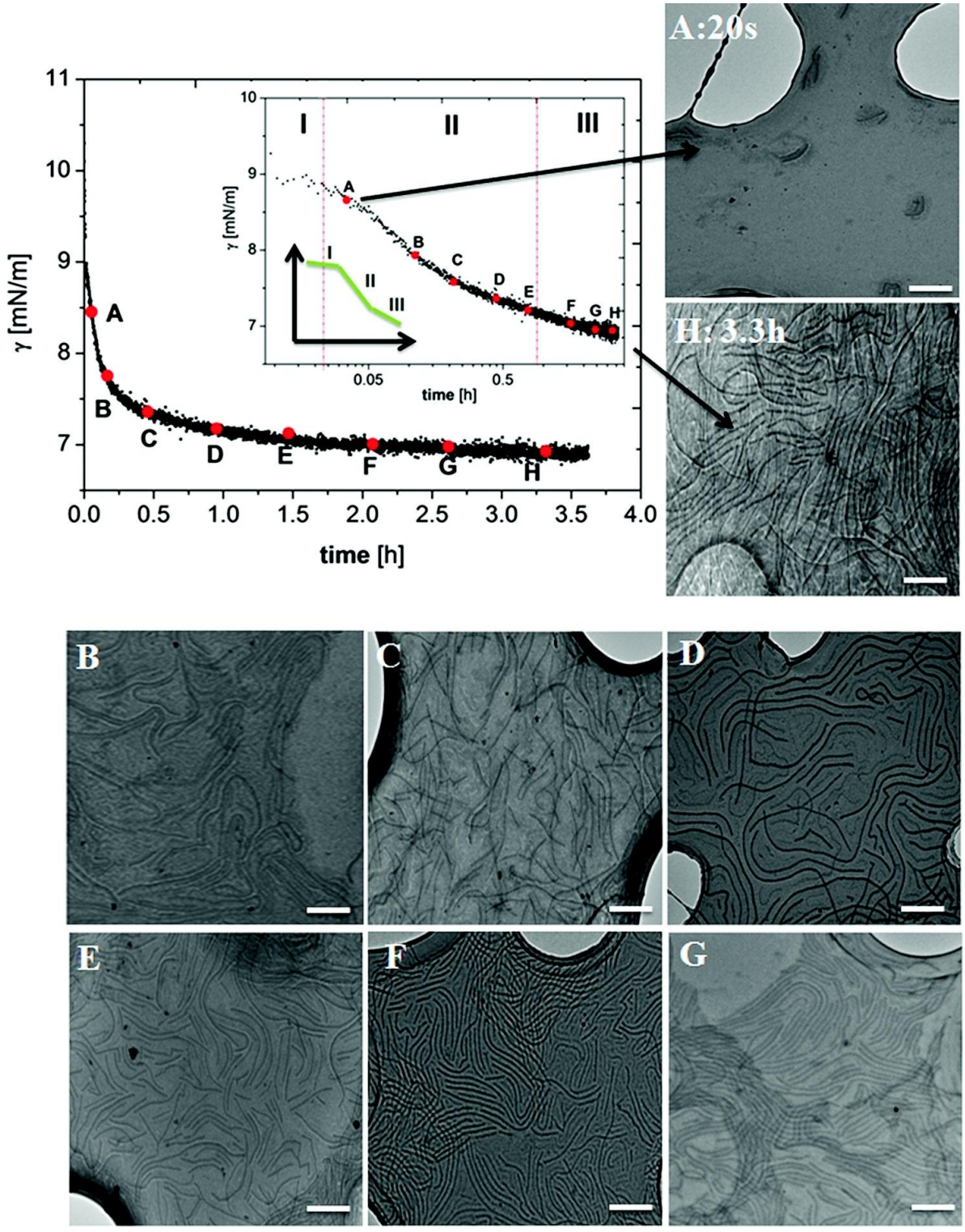

Fig. 11:

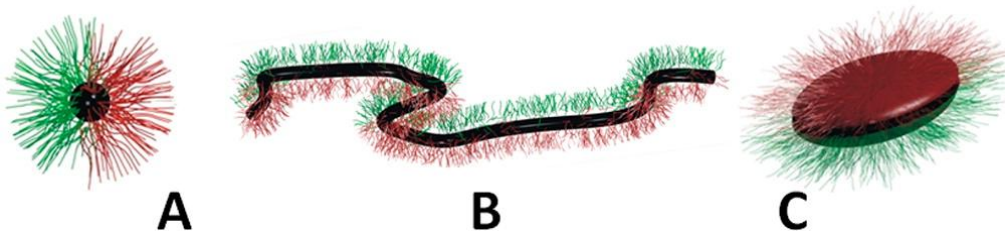
A
B
C

Fig. 12:

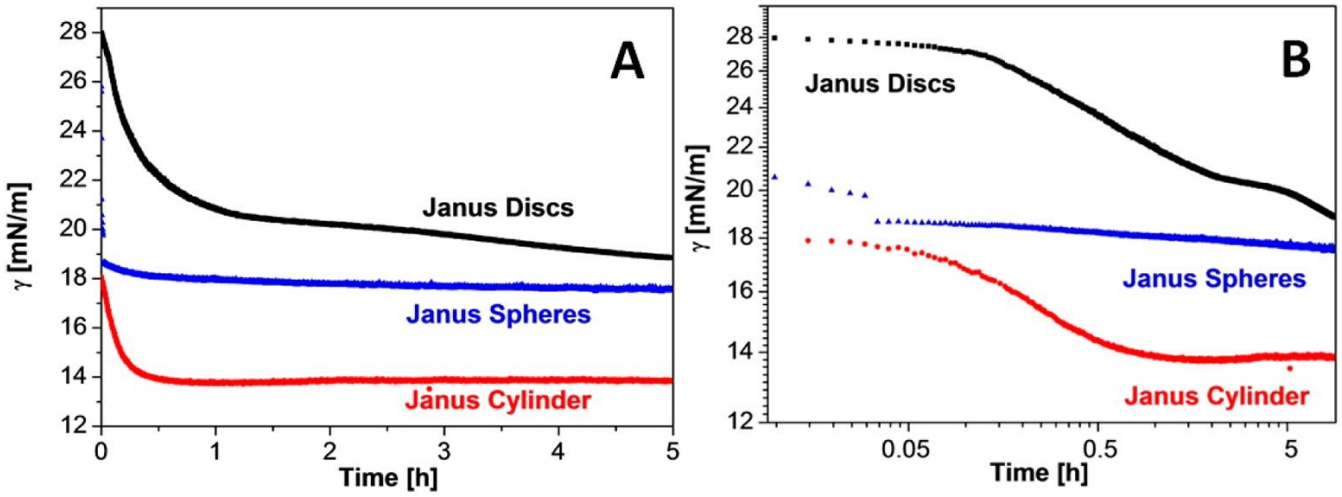
A
Janus Discs
Janus Spheres
Janus Cylinder
γ [mN/m]
Time [h]
B
Janus Discs
Janus Spheres
Janus Cylinder
γ [mN/m]
Time [h]

Fig. 13:

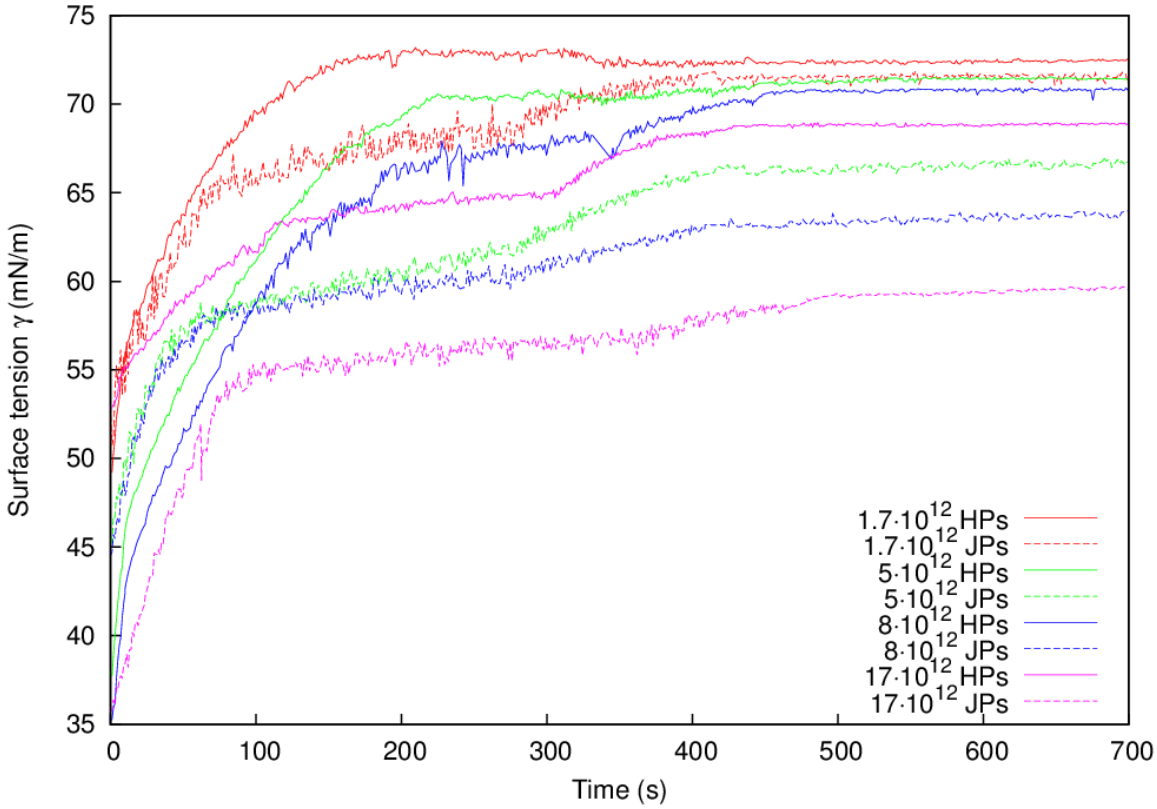
Surface tension γ (mN/m)
Time (s)
75
70
65
60
55
50
45
40
35
0
100
200
300
400
500
600
700
1.7·10^12 HPs
1.7·10^12 JPs
5·10^12 HPs
5·10^12 JPs
8·10^12 HPs
8·10^12 JPs
17·10^12 HPs
17·10^12 JPs

Fig. 14:

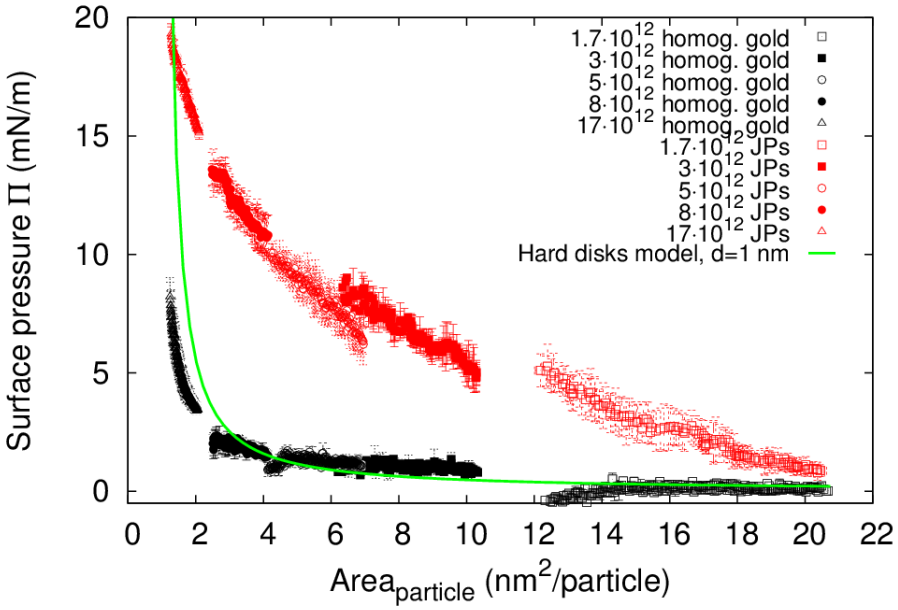

(a) Water/air interface.

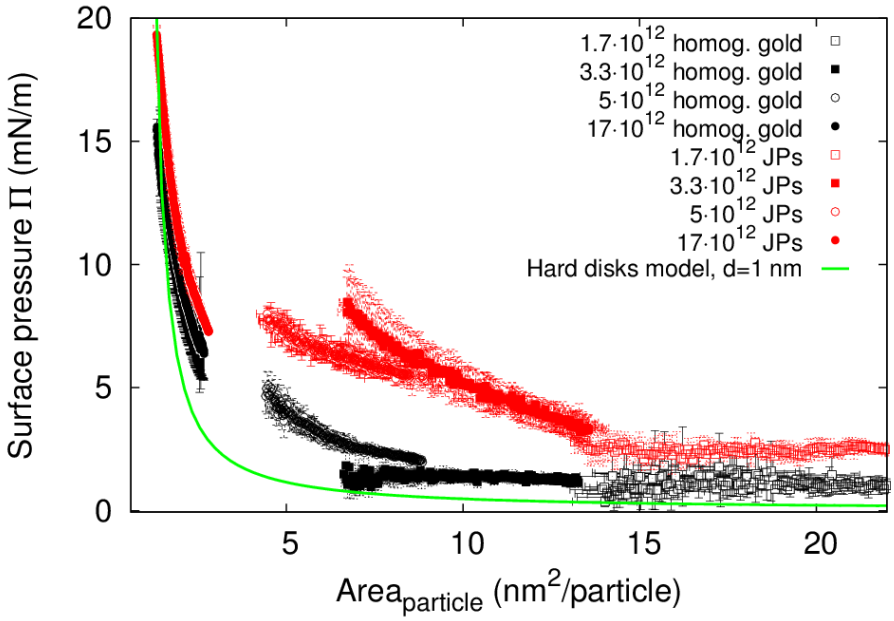

(b) Water/decane interface.

Fig. 15:

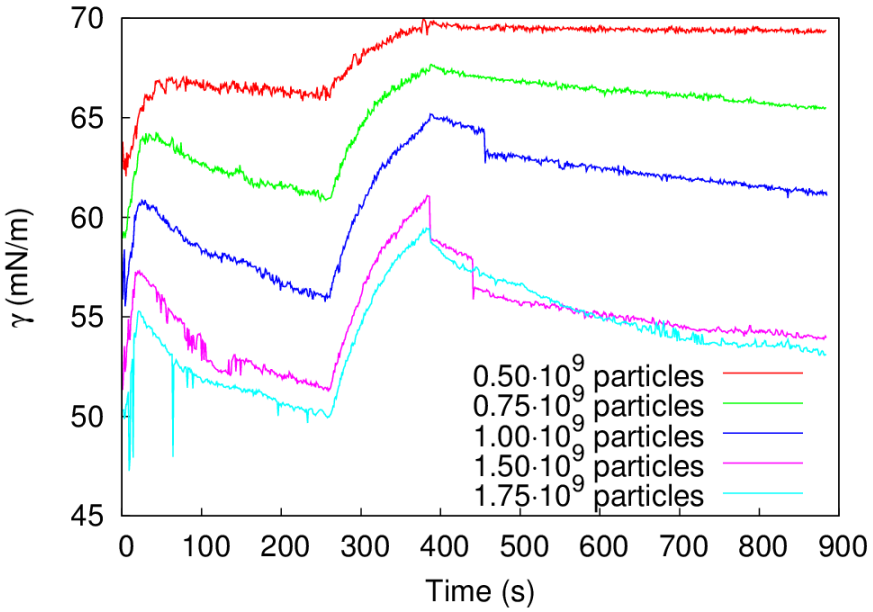
70
65
60
55
50
45
γ (mN/m)
0
100
200
300
400
500
600
700
800
900
Time (s)
0.50·10^9 particles
0.75·10^9 particles
1.00·10^9 particles
1.50·10^9 particles
1.75·10^9 particles

Fig. 16:

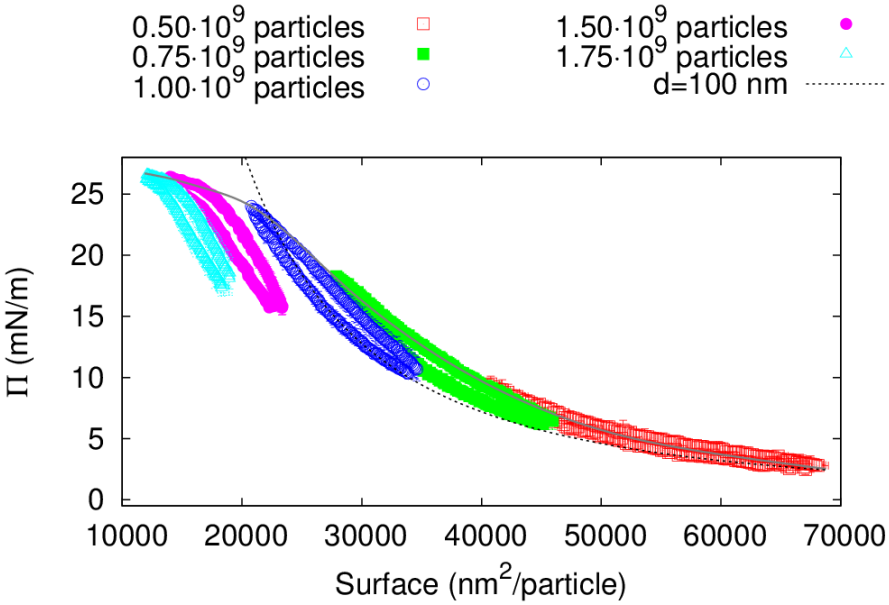
0.50·10^9 particles
0.75·10^9 particles
1.00·10^9 particles
1.50·10^9 particles
1.75·10^9 particles
d=100 nm
25
20
15
10
5
0
Π (mN/m)
10000
20000
30000
40000
50000
60000
70000
Surface (nm^2/particle)